Cancer Research

YAP1-Mediated Suppression of USP31 Enhances NFκB Activity to Promote Sarcomagenesis

Shuai Ye[1], Matthew A. Lawlor[2], Adrian Rivera-Reyes[1], Shaun Egolf[1], Susan Chor[1], Koreana Pak[1], Gabrielle E. Ciotti[1], Avery C. Lee[1], Gloria E. Marino[1], Jennifer Shah[1], David Niedzwicki[1], Kristy Weber[3], Paul M.C. Park[2], Md. Zahidul Alam[1], Alison Grazioli[4], Malay Haldar[1], Mousheng Xu[2], Jennifer A. Perry[2], Jun Qi[2,5], and T.S. Karin Eisinger-Mathason[1]

Abstract

To date, no consistent oncogenic driver mutations have been identified in most adult soft tissue sarcomas; these tumors are thus generally insensitive to existing targeted therapies. Here we investigated alternate mechanisms underlying sarcomagenesis to identify potential therapeutic interventions. Undifferentiated pleomorphic sarcoma (UPS) is an aggressive tumor frequently found in skeletal muscle where deregulation of the Hippo pathway and aberrant stabilization of its transcriptional effector yes-associated protein 1 (YAP1) increases proliferation and tumorigenesis. However, the downstream mechanisms driving this deregulation are incompletely understood. Using autochthonous mouse models and whole genome analyses, we found that YAP1 was constitutively active in some sarcomas due to epigenetic silencing of its inhibitor angiomotin (AMOT). Epigenetic modulators vorinostat and JQ1 restored AMOT expression and wild-type Hippo pathway signaling, which induced a muscle differentiation program and inhibited sarcomagenesis. YAP1 promoted sarcomagenesis by inhibiting expression of ubiquitin-specific peptidase 31 (USP31), a newly identified upstream negative regulator of NFκB signaling. Combined treatment with epigenetic modulators effectively restored USP31 expression, resulting in decreased NFκB activity. Our findings highlight a key underlying molecular mechanism in UPS and demonstrate the potential impact of an epigenetic approach to sarcoma treatment.

Significance: A new link between Hippo pathway signaling, NFκB, and epigenetic reprogramming is highlighted and has the potential for therapeutic intervention in soft tissue sarcomas. *Cancer Res; 78(10); 2705–20. ©2018 AACR.*

Downloaded from http://aacrjournals.org/cancerres/article-pdf/78/10/2705/2764759/2705.pdf by guest on 27 August 2022

Introduction

Soft tissue sarcomas are a heterogeneous group of mesenchymal malignancies arising in muscle, fat, cartilage, and connective tissues (1, 2). Whereas loss or mutation of tumor suppressors (i.e., p53) occurs in approximately 50% of sarcomas (3, 4), sequencing of common adult sarcoma subtypes including fibrosarcoma, liposarcoma, and undifferentiated pleomorphic sarcoma (UPS) have produced no evidence of consistent oncogenic driver mutations (4). The lack of targetable oncogenes has stalled the development of therapeutic modalities (5, 6). We focused our efforts on skeletal muscle UPS given its particularly aggressive nature, lack of nonsurgical treatment strategies, and its high frequency of diagnoses relative to other adult subtypes.

We previously reported that deactivation of the Hippo pathway, a signaling cascade that negatively regulates cell proliferation, promotes sarcomagenesis in skeletal muscle–derived UPS (7). Furthermore, genome-wide analysis of The Cancer Genome Atlas (TCGA) sarcoma dataset confirmed that deregulated Hippo signaling is a contributing factor in sarcomagenesis (2). Inactivation of the Hippo pathway stabilizes the transcriptional effector, YAP1, allowing it to translocate to the nucleus and promote a pro-proliferation gene expression program. Inhibition of YAP1 reduces proliferation in multiple sarcoma subtypes, including UPS, although no genetically engineered mouse model (GEMM) of Yap1-deficient UPS existed prior to this study. While YAP1 activity has been implicated in multiple sarcoma subtypes (7–10), its exact function, regulation, and targets in this context are unclear.

The precise cell of origin for UPS is not known (11). However, in skeletal muscle, these tumors are thought to arise from muscle progenitor cells/satellite cells (12). Whereas investigation of the Hippo pathway in muscle-derived sarcomas has been limited to rhabdomyosarcoma (13), in normal myoblasts, persistent elevated YAP1 and NFκB signaling facilitates proliferation and inhibits differentiation (13–15).

In addition to Hippo pathway deregulation, several studies have recently shown that alterations in the epigenetic landscape can promote sarcomagenesis. Specifically, certain pediatric

[1]Abramson Family Cancer Research Institute, Department of Pathology & Laboratory Medicine, Penn Sarcoma Program, University of Pennsylvania Perelman School of Medicine, Philadelphia, Pennsylvania. [2]Department of Cancer Biology, Dana-Farber Cancer Institute, Boston, Massachusetts. [3]Department of Orthopedic Surgery, Penn Sarcoma Program, University of Pennsylvania Perelman School of Medicine, Philadelphia, Pennsylvania. [4]Department of Medicine, University of Maryland School of Medicine, Baltimore, Maryland. [5]Department of Medicine, Harvard Medical School, Boston, Massachusetts.

Note: Supplementary data for this article are available at Cancer Research Online (http://cancerres.aacrjournals.org/).

Corresponding Authors: T.S. Karin Eisinger-Mathason, Abramson Family Cancer Research Institute, University of Pennsylvania, 414 BRB II/III, 421 Curie Boulevard, Philadelphia, PA 19104-6160. Phone: 215-898-9086; Fax: 215-746-5511; E-mail: karineis@pennmedicine.upenn.edu; and Jun Qi, Department of Cancer Biology, Dana-Farber Cancer Institute, Department of Medicine, Harvard Medical School, Boston, MA 02215. E-mail: Jun_qi@dfci.harvard.edu

doi: 10.1158/0008-5472.CAN-17-4052

©2018 American Association for Cancer Research.

sarcomas are linked to chromosomal translocations of transcription factor loci encoding chromatin-remodeling factors (16, 17). Copy number loss of chromatin modulators have also been found in some subtypes (15). Together, these studies suggest that disruption of chromatin architecture may be a common event in sarcomagenesis. Our recent work showed that treatment with the histone deacetylase (HDAC) inhibitor vorinostat, also known as suberoylanilide hydroxamic acid (SAHA), leads to reexpression of *HIF2α* and a corresponding 50% reduction in UPS sarcomagenesis *in vivo* (18). These findings support the hypothesis that epigenetic modulation can reduce tumorigenesis by returning key transcription factors to the expression and activity levels found in quiescent cells.

In this study, we utilized human skeletal muscle UPS samples and the autochthonous mouse model of UPS to determine that YAP1 promotes proliferation and dedifferentiation through persistent hyperactivation of NFκB. Analysis of the chromatin state in human UPS revealed the presence of massive enhancers, or super enhancers, notably at NFκB target gene loci. Using the epigenetic modulators vorinostat/SAHA and JQ1 (BET bromodomain protein inhibitor), we found that tumor growth was reduced secondary to Hippo pathway reactivation and loss of YAP1 expression. Furthermore, we found that YAP1 suppresses expression of ubiquitin specific peptidase 31 (USP31), a newly identified negative regulator of NFκB signaling (19), resulting in uncontrolled proliferation and tumorigenesis. YAP1 inhibition restored expression of USP31, indicating that aberrant stabilization of YAP1 promotes NFκB activity. We conclude that epigenetic therapy can reclaim control of YAP1-mediated NFκB signaling and subsequently inhibit tumor cell proliferation, induce differentiation, and decrease sarcomagenesis *in vivo*.

Materials and Methods

Mouse models

GEMM. All experiments were performed in accordance with NIH guidelines and were approved by the University of Pennsylvania Institutional Animal Care and Use Committee. We generated $Kras^{G12D+}$; $Trp53^{fl/fl}$; $Yap1^{fl/fl}$ (KPY) mice by crossing KP and $YAP1^{fl/fl}$ animals. Tumors were generated by injection of a calcium phosphate precipitate of adenovirus expressing Cre recombinase (University of Iowa, Iowa City, IA) into the right gastrocnemius muscle of 3- to 6-month-old mice.

Allograft mouse model. For subcutaneously implanted tumors, 1×10^6 KP230 cells were injected subcutaneously into the flanks of 6-week-old nu/nu mice (Charles River Laboratories). Animals were euthanized after 14 days of JQ1 peritoneal injection. For Rela-mediated knockdown KP230 allografts, 1×10^6 cells were injected into the flanks of mice with control tumor cells (scrambled shRNA) and experimental tumor cells (Rela shRNA). Tumor size was measured every other day, and animals were euthanized after 21 days posttumor cells' injection. Tumor volume was calculated by using the formula $(ab^2)\pi/6$, where a is the longest measurement and b is the shortest.

In vivo drug treatment. For *in vivo* drug studies, total 44 ($n = 11$ per group) autochthonous KP mice were randomly divided into 4 groups to receive different treatments once tumors reached 100 mm^3, and injected for up to 20 days. The mice were euthanized 24 hours after the tumor volume reached 2,000 mm^3): (i) Vehicle group (10% Hydroxypropyl-β-cyclodextrin plus DMSO was diluted daily in sterile 45% PEG/55% H_2O); (ii) JQ1 group (JQ1 was diluted daily in 10% HP-β-CD injected into the peritoneal cavity 25 mg/kg twice daily); (iii) SAHA group (SAHA was diluted in sterile 45% PEG/55% H_2O injected into the peritoneal cavity 50 mg/kg daily); (iv) JQ1 and SAHA combination treatment group (drugs were diluted in its vehicles, respectively). Treatment method for drug combination group: (i) 25 mg/kg SAHA + 50 mg/kg JQ1 for first 5 days; (ii) 25 mg/kg SAHA + 25 mg/kg JQ1 each other day for 10 days; (iii) 25 mg/kg SAHA + 50 mg/kg JQ1 for 2 days; and (iv). then mice with tumors received 25 mg/kg SAHA with 25 mg/kg JQ1 for 3 days. Mice without tumors received 5 mg/kg SAHA and 5 mg/kg JQ1 for 3 days. JQ1 was provided by J. Qi (Dana-Farber Cancer Institute, Boston, MA) and SAHA was purchased from Cayman Chemical. HP-β-CD and PEG400 were obtained from Sigma-Aldrich.

Cell lines. Human HT-1080 (fibrosarcoma), RD (rhabdomyosarcoma), LPS224 and LPS863 (liposarcoma), SKLMS1 and SKUT1 (leiomyosarcoma), and HEK-293T cell lines were purchased from ATCC. STS-109 and STS-48 cell lines were derived from human UPS patients, then validated by Dr. Rebecca Gladdy (Sinai Health System, Toronto, Ontario, Canada). KP230 and KIA cell lines were derived from UPS mouse tumors as described in Eisinger-Mathason and colleagues (4). Short tandem repeat analysis was performed at the time of derivation and confirmed in April 2015. Cells were purchased, thawed, and then expanded in the laboratory. Multiple aliquots were frozen within 10 days of initial resuscitation. For experimental use, aliquots were resuscitated and cultured for up to 20 passages (4–6 weeks) before being discarded. Cells were cultured in DMEM with 10% (v/v) FBS and 1% penicillin/streptomycin. All cell lines were confirmed to be negative for mycoplasma contamination.

Lentiviral transduction. shRNA-mediated knockdown of AMOT TRCN: 0000166812, 0000165373, 0000162009, 0000159177, 0000162010; Amot TRCN: 00001266880, 0000126883, 0000349515, 0000126881, 0000317410. Yap1 TRCN: 0000095864, 0000095867, 0000095868; YAP1 TRCN: 0000107266, 0000107267, 0000015547; Usp31 TRCN: 0000092218, 0000092219, 0000092220, 0000092221, 0000092222, Rela (p65 NFκB) TRCN: 0000055343, 0000055344, 0000055346, 0000055347, and Scramble shRNA were obtained from Addgene. shRNA plasmids were packaged by using the third-generation lenti-vector system (VSV-G, p-MDLG, and pRSV-REV) and expressed in HEK-293T cells. Supernatant was collected at 24 and 48 hours after transfection and subsequently concentrated by using 10-kDa Amicon Ultra-15 centrifugal filter units (Millipore). Lenti GFP-AMOT p130 (plasmid 32828), Lenti GFP-AMOT p130 Y242/287A (plasmid 32829), YAP1-V5 (plasmid 42555), and YAP1 (S6A)-V5 (plasmid 42562) were purchased from Addgene. pLX304 vector was obtained from Addgene. Lenti-pcdh-EF1 and Lenti-pcdh-GFP were used as the empty vector control in our laboratory.

IHC. Twenty human UPS paraffin-embedded tissues obtained from the Surgical Pathology group at University of Pennsylvania (Philadelphia, PA) were stained for both p-p65 and Yap1. IHC was performed on 5-μm tissue sections according to standard protocols. Slides were digitally scanned by the Pathology Core Laboratory at the Research Institute at the Children's Hospital of

Downloaded from http://aacrjournals.org/cancerres/article-pdf/78/10/2705/2764759/2705.pdf by guest on 27 August 2022

Philadelphia (Philadelphia, PA). The software of Aperio ImageScope (Leica Biosystems) was used for the quantification of slides. Modified macro (Nuclear v9 parameter) was used to distinguish the intensity of staining. The following antibody concentrations were used: rabbit anti-YAP1 (4912; 1:100; Cell Signaling Technology), anti-phospho p65 (86299; 1:250; Abcam) rabbit anti-Ki-67 (15580; 1:100; Abcam), rabbit anti-MYOD (18943-1-AP; 1:100; Proteintech). IHC of human soft tissue sarcoma and smooth/skeletal muscle samples was performed by using core biopsy arrays (US Biomax, #SO801a). Images were taken by Leica 500 microscope and analyzed by using Photoshop CS3 (Adobe Systems). For quantification, 5 areas of tumor and 5 areas of adjacent muscle (identified by hematoxylin and eosin staining) were captured per section and averaged to determine the mean % positive nuclei/section.

Immunoblots. Protein lysate was prepared in SDS/Tris (pH 7.6) lysis buffer, separated by electrophoresis in 8%–10% SDS/PAGE gels, transferred to nitrocellulose membrane, and probed with the following antibodies: rabbit anti-YAP1 (4912; 1:1,000), rabbit anti-p-Yap (Ser397; 13619; 1:1,000), rabbit anti-GAPDH (2118; 1:1,000), mouse anti-AMOT (60156-1-lg 1:500), rabbit anti-V5-tag (13202; 1:1,000), rabbit anti-p65 (8242; 1:500), rabbit anti-p-p65 (Ser536; 3033; 1:500), rabbit anti-caspase-3 (9662; 1:1,000), rabbit anti-HSP90 (4875; 1:1,000; Cell Signaling Technology), rabbit USP31 (12076-1-AP; 1:1,000), rabbit anti-MYOD1 (18943-1-AP; 1:500; Proteintech), rabbit FOXM1 (sc-502; 1:500; Santa Cruz Biotechnology), c-Myc (32072; 1:2,000), p57 Kip2 (75974; 1:500; Abcam), mouse anti-Lamin B2 (D18; University of Iowa Developmental Studies Hybridoma Bank). SuperSep Phos-tag gel was purchased from Wako. Rabbit anti-LATS1 (3477; 1:1,000), rabbit anti-MST1 (3682; 1:1,000), and rabbit anti-MST2 (3952; 1:1,000; Cell Signaling Technology) were used to detect phosphorylated proteins.

Luciferase assay. Plasmid pHAGE NFκB-TA-LUC-UBC-GFP-W (49343; Addgene) was transfected into 293T cells (ATCC) to generate lentiviral particles in the supernatant. Viral supernatant was harvested and then concentrated by centrifugal filter units (Amicon Ultra-15, Millipore). NFκB reporter virus was transduced into KP230 cells. GFP-positive NFκB reporter cells were sorted generating an approximately 85% pure GFP^+ cell line. For shRNA assays, the NFκB the reporter cell line was transduced with lentivirus expressing control, Usp31, or Yap1 shRNA. For drug studies, the NFκB reporter cells were treated with SAHA (2 μmol/L)/JQ1 (0.5 μmol/L) and BAY 11-7085 (1.5 μmol/L, Selleckchem) for 48 hours. Twelve hours prior to detecting luciferase activity, TNFα (10 ng/mL, R&D Systems) was added. Luciferase activity was assayed using the Dual Luciferase Assay System (E2920, Promega) according to the manufacturer's protocol on a Luminometer (GLOMAX, Promega). Results were calculated as fold induction.

Oncomine and TCGA survival analysis. We used the publicly available database Detwiller and colleagues through Oncomine Research Premium edition software (version 4.5, Life Technologies) to query *AMOT* expression in sarcomas and normal tissues. *YAP1*, *MYC*, and *PHLDA1* gene expression were correlated with overall survival in patients with MFH/UPS and DDLS, using the TCGA sarcoma dataset. Kaplan–Meier analyses were performed for overall survival of patients.

Microarray-based gene set enrichment analysis. Differential gene expression was tested using significance analysis of microarrays (SAM, samr v2.0), yielding fold change, q-value (false discovery rate) and d-score for each gene. We observed a small number of genes meeting our cutoffs for differential expression and so proceeded to GSEA. Log_2-transformed RMA-sst expression values were used as input to GSEA (20) where enrichment was tested against the hallmark gene sets from the Molecular Signatures Database (MSigDB, v5.1, http://software.broadinstitute.org/gsea/msigdb/index.jsp).

C2C12 growth and differentiation. C2C12 murine myoblast cells were obtained from ATCC. The cells grow as undifferentiated myoblasts in growth medium (20% FBS with 1% penicillin/streptomycin), and were passaged every 2–3 days at 50% subconfluence. To induce differentiation, cells were grown overnight to approximately 80% confluence in growth medium, and then switched to DMEM supplemented with 2% horse serum. Differentiation media were refreshed every 2 days.

ChIP-seq and RNA sequencing

ChIP-seq. For tumor samples resected from UPS patients at the Hospital of the University of Pennsylvania, approximately 100 mg of tissue was minced into 1–2 mm pieces and incubated in 1% formaldehyde for 15 minutes. Formaldehyde was quenched with glycine at 0.125 mol/L. Fixed tissue was homogenized for 60 seconds with a Tissue Tearor Homogenizer (Biospec) at 30,000 rpm. Homogenized tissue was washed with ice-cold PBS with 1× HALT protease inhibitor. For cell line ChIP-RX, samples were fixed for 10 minutes in 1% formaldehyde quenched with glycine and washed with PBS as above. 5e6 S2 cells (*Drosophila melanogaster*) were added to each sample of 2.5e7 for ChIP-RX normalization in downstream analysis.

RNA-sequencing. Tissue preprocessed via mortar and pestle homogenization or 2.5e5 cells were homogenized via Qiashredder column (Qiagen). Samples were then processed via mRNeasy Mini Kit (Qiagen). RNA sequencing (RNA-seq) datasets in fastq format were fed into RSEM for mRNA sequence alignment and quantification (21). Gene counts generated by RSEM were fed into edgeR (22) to compute log fold change (logFC) and *P* value. False discovery rate is used for multiple comparison correction. The GSEA software and Hallmark gene sets (20) were used for GSEA. Genes were ranked by rank score $-\log(P) \times \text{sign}(\text{logFC})$.

Statistical analysis

Statistical analysis was performed using Prism (GraphPad software). Data are shown as mean ± SEM or SD. Data are reported as biological replicates, with technical replicates indicated in figure legends. Student *t* tests (unpaired two-tailed) were performed to determine whether a difference between two values is statistically significant different, with $P < 0.05$ considered significant. *In vitro* assays were performed in triplicate unless otherwise stated.

Accession codes

Sequencing data reported in this article have been deposited in NCBI's Gene Expression Omnibus and are accessible through GEO Series accession number GSE97295, GSE97296, GSE97297, GSE109920, and GSE109923.

Downloaded from http://aacrjournals.org/cancerres/article-pdf/78/10/2705/2764759/2705.pdf by guest on 27 August 2022

Results

YAP1 regulates NFκB target expression in murine UPS

Deregulation of the Hippo pathway is associated with muscle-derived sarcoma subtypes but the downstream mechanisms are unclear (7, 8, 23). Although we have access to only a small number of TCGA patient samples, which prevents our analysis from reaching statistical significance, expression of YAP1 strikingly correlates with long-term survival in human UPS patients (Fig. 1A). To determine the relevance of these findings, we evaluated YAP1 expression in a variety of sarcomas by IHC of a human biopsy tissue microarray. YAP1 expression is particularly high in muscle UPS (Fig. 1B, group 2, boxed), compared with normal mesenchymal tissues including skeletal and smooth muscle (Fig. 1B, group 1). The clinical details of each sample can be found in Supplementary Fig. S1A. To test the role of YAP1 in UPS, we introduced *Yap1*$^{fl/fl}$ alleles into our *LSL-Kras*$^{G12D/+}$; *Trp53*$^{fl/fl}$ (KP) GEMM of skeletal muscle UPS to generate *LSL-Kras*$^{G12D/+}$; *Trp53*$^{fl/fl}$;*Yap1*$^{fl/fl}$ (KPY) animals. Tumors are generated by injection of adenovirus expressing Cre recombinase into the right gastrocnemius muscle. The Cre recombinase activates expression of oncogenic Kras and deletes p53 expression in infected muscle progenitor cells (24, 25). Although *Kras* mutation is rare in sarcomas, *Trp53* mutation and deletion are very common (2). Furthermore, hyperactivation of the MAPK pathway, downstream of KRAS activation, is common in UPS and is an excellent prognostic indicator for recurrence (26). This model and a similar one, *Kras*$^{G12D/+}$; *Ink4a/arf*$^{fl/fl}$ (KIA), generate sarcomas that are histologically, transcriptionally, and morphologically identical to UPS and are thus the standard GEMMs in UPS studies (24, 25). Yap1 protein expression is stabilized in KP tumors providing further rationale for the study of Yap1 function in sarcoma using this model (Fig. 1C and D). Loss of Yap1 in KPY tumors was confirmed by Western blot and IHC analyses (Fig. 1C and D; Supplementary Fig. S1B). KP tumors were initially palpated at day 45 post-Adeno-cre injections and were collected when they reached 2 cm^3 (maximum tumor volume). KPY tumors were harvested either when they reached 2 cm^3 or 60 days post Adeno-cre injection, the time-point at which all KP mice had reached maximum tumor volume. Deletion of *Yap1* delayed tumor initiation (median latency KP: 57 days; KPY: 59 days, $P < 0.0001$) and growth (Fig. 1E–H). Several KPY mice never developed visible tumors and those animals are represented in Fig. 1E with a data point at day 65. Proliferation was reduced by approximately 50% in KPY tumors as defined by Ki67 positivity (Fig. 1D; Supplementary Fig. S1C). To determine the functional role of Yap1 in UPS, we performed microarray analysis of 5 individual KP and KPY tumors. Gene set enrichment analysis (GSEA) revealed that "TNFα-induced NFκB" signaling is significantly reduced in KPY tumors (Fig. 1I and J). Furthermore, using the TCGA sarcoma dataset, we determined that the YAP1-dependent NFκB target *PHLDA1* is associated with poor survival in UPS (Fig. 1K). The specific effects of YAP1 on Tnfα-mediated signaling suggest high levels of Tnfα cytokine production in the UPS tumor microenvironment, which activates downstream NFκB signaling. To validate Tnfα expression in UPS tumor tissue, and to determine the source of Tnfα production, we fractionated KP tumors and isolated tumor-associated macrophages (TAM), which are known to produce significant amounts of Tnfα. We compared Tnfα expression in isolated KP tumor cells and TAMs. Tnfα mRNA expression was approximately 45-fold higher in TAMs than in tumor cells (Fig. 1L, left). To determine whether the relative expression of Tnfα in KP TAMs was physiologically significant, we compared this *in vivo* induction with that of the classical *in vitro* model of LPS-stimulated murine bone marrow–derived macrophages (BMDM). LPS-stimulated BMDMs express approximately 100 fold more Tnfα than untreated BMDMs (Fig. 1L, right). Together, these data suggest that KP TAMs produce a physiologically relevant amount of Tnfα, which could easily activate NFκB signaling. However, NFκB signaling may be activated by additional mechanisms in this context.

We tested the ability of Yap1 to control NFκB activity *in vitro* using an established luciferase reporter assay (27). Sarcoma cells derived from a KP tumor were infected with a GFP-labeled NFκB reporter construct, sorted to approximately 86% purity, and then infected with lentivirus expressing control or *Yap1* shRNA. NFκB activity is reduced by approximately 50% in *Yap1* shRNA–expressing cells, treated with Tnfα, compared with treated control shRNA-expressing cells (Fig. 1M). From these findings we conclude that YAP1 promotes NFκB activity, which may enhance sarcomagenesis.

Hyperactivation of NFκB super enhancers in human UPS

To determine the extent of NFκB signaling in human UPS, we performed multiple genome-wide analyses of these tumor samples directly from patients. We performed acetylated histone 3 lysine 27 (H3K27Ac) chromatin immunoprecipitation with massively parallel DNA sequencing [chromatin immunoprecipitation sequencing (ChIP-seq)] using three independent UPS patient samples originating in skeletal muscle tissue (Supplementary Fig. S2A). Acetylation of lysine residues on histone tails is linked to active euchromatin transcription, especially at H3K27Ac, which is associated with active *cis*-regulatory elements (28). Therefore, high levels of H3K27Ac at the enhancer regions of NFκB target genes are directly associated with elevated NFκB activity. The observed genome-wide binding of H3K27Ac antibody was consistent in all three UPS samples. We then conducted focused epigenomic analysis on regions of dramatic H3K27Ac enrichment, frequently referred to as super enhancer (SE) analysis, across all three samples to map the regions of highly active enhancers across the whole genome, and identify regions of differential hyperacetylation (SE; Fig. 2A). We identified activation of multiple SE regions associated with NFκB from the set of overall SEs. The SEs associated with NFκB pathway genes correlated well with average H3K27Ac signal density in representative human UPS at SEs (Fig. 2B and C). More convincingly, NFκB pathway components, such as *RELA*, *BCL3*, and *RELB* showed enhanced H3K27Ac signal in all three UPS samples (Fig. 2D–F), the input data are listed in Supplementary Fig. S2B and S2D, and the identified SEs were most significantly associated with the hallmark M5890 gene set referred to as "TNFA signaling via NFκB" (Fig. 2G–I) in all three human samples. As a control assay for H3K27Ac ChIP-Seq, we performed RNA-seq on human UPS tumor sample #1 compared with normal adult skeletal muscle. Using differential gene expression analysis (29), we observed that TNFα and NFκB pathway genes, including *RELA* itself, were significantly upregulated in UPS, while the muscle differentiation markers, *MEF2C* and *MYOD1*, were contrastingly downregulated (Fig. 2J, enlarged in Supplementary Fig. S2E). Likewise, we noted high expression of NFκB targets in UPS, including many of those identified as YAP1-regulated in the KP/KPY microarray [i.e., *CCL2* (30), *BCL3* (31), *PHLDA1* (32); Fig. 1I]. Furthermore, GSEA

Downloaded from http://aacrjournals.org/cancerres/article-pdf/78/10/2705/2764759/2705.pdf by guest on 27 August 2022

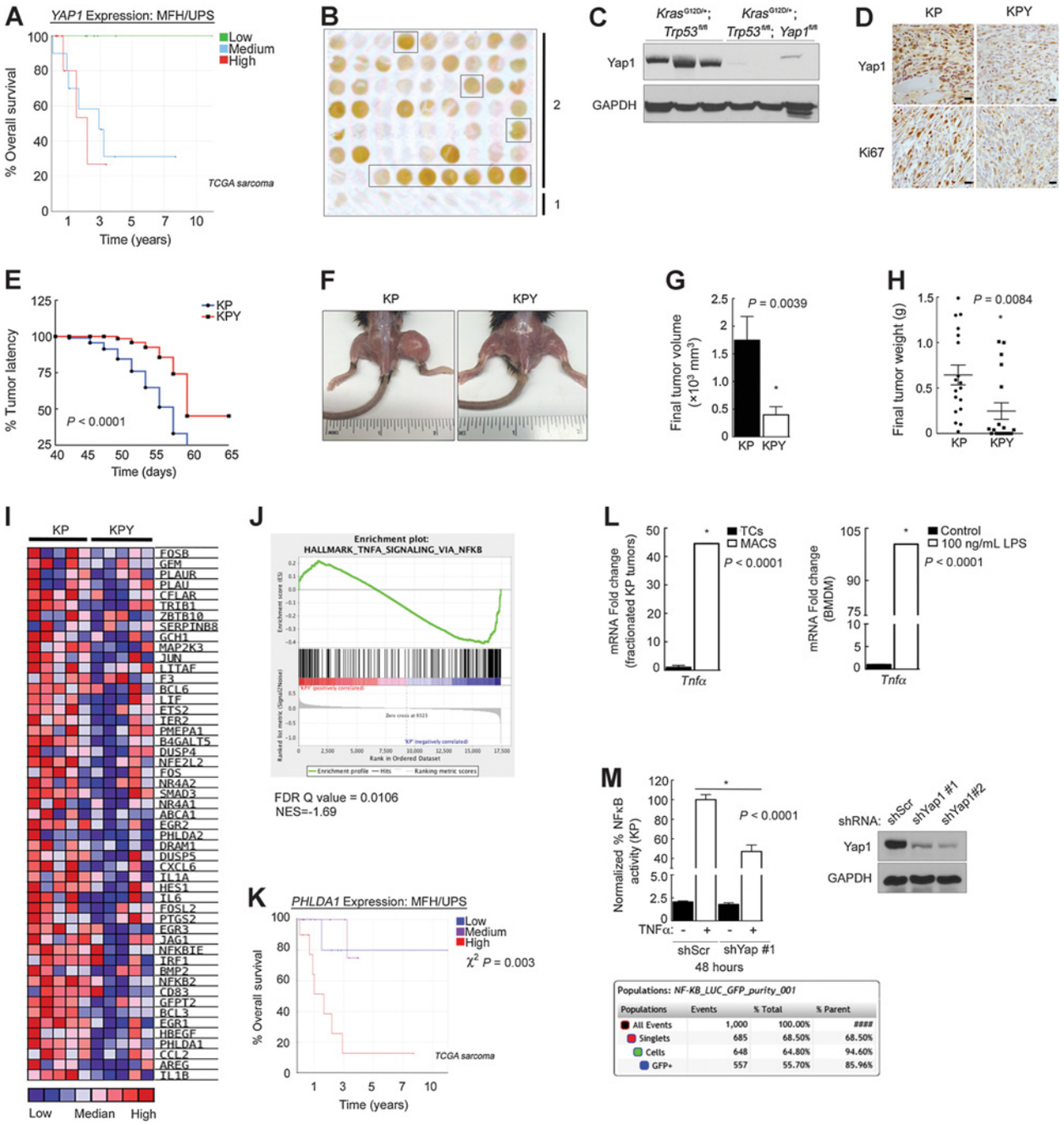

Figure 1.

YAP1 promotes sarcomagenesis and NFκB activity. **A,** Kaplan–Meier curve of overall survival of MFH/UPS patients ($n = 29$; TCGA sarcoma dataset). **B,** IHC of patient tissue microarray; Group 1, normal skeletal muscle, smooth muscle, arterial tissue etc.; Group 2, sarcomas black box indicates UPS. **C,** *Kras*$^{G12D/+}$; *Trp53*$^{fl/fl}$ model of UPS; Western blot analysis of YAP1 from three independent KP and KPY tumors. **D,** IHC of KP and KPY tumors. Scale bar, 100 μm. **E,** *Yap1* deletion in KP ($n = 20$ mice per group from two independent cohorts). **F,** Images of KP and KPY tumors. Tumor volume (**G**) and tumor weight (**H**) in KP and KPY. SEM, 1 true outlier (GraphPad Quick Calcs, outlier calculator) removed from each group. **I,** Heatmap of microarray analysis of five independent KP and KPY tumors. **J,** GSEA of microarray from **I** using the "Hallmark TNFα signaling via NFκB" gene set. **K,** Kaplan–Meier curve of overall survival of UPS patients based on *PHLDA1* expression. **L,** mRNA from macrophages (MACS; left) and tumor cells (TCs) from KP tumors. Right, LPS-stimulated (100 ng/mL; 24 hours) BMDM *in vitro*; SD. **M,** Left, NFκB luciferase assay in KP cells; SD. Top right, KP cells expressing control or two independent *Yap1* shRNAs. Bottom, cell sorting report indicating that the GFP-luciferase construct was present in approximately 86% of cells.

Downloaded from http://aacrjournals.org/cancerres/article-pdf/78/10/2705/2764759/2705.pdf by guest on 27 August 2022

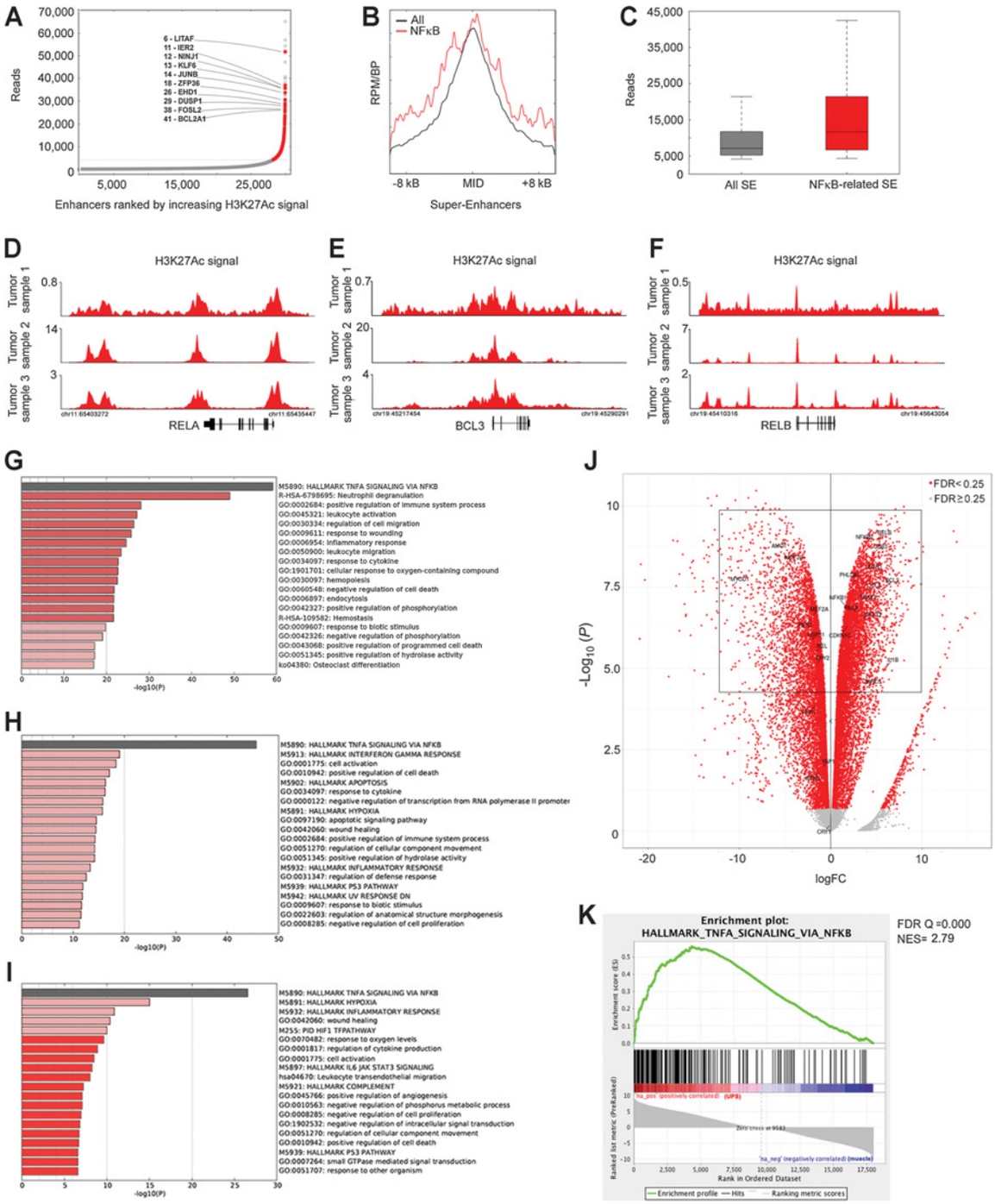

Figure 2.

ChIP-seq (H3K27Ac) and super-enhancer analysis of human UPS patient samples. **A,** Ranked plots of enhancers defined in three primary human UPS tumors ranked by increasing H3K27Ac ChIP-seq signal (average reads). SE-associated genes from the "Hallmark TNFα signaling via NFκB" gene set are highlighted in red. **B,** Meta gene representation of H3K27Ac ChIP-seq read density (rpm/bp) at NFκB associated SEs (red line) compared with all SEs (black line). The *x*-axis shows the start and end of the SE regions flanked by ± 10 kb of adjacent sequence. **C,** Boxplot quantification of genes (reads) closest to NFκB associated SEs compared with all other SEs. $P = 4.25 \times 10e6$ (Welch two-tailed *t* test). **D–F,** Gene tracks of H3K27ac ChIP-seq signal (rpm/bp) for H3K27ac at the *RELA* (**D**), *BCL3* (**E**), and *RELB* (**F**) regions. **G–I,** Pathway enrichment analysis (via Metascape) of genes associated with SEs called via meta-analysis of three primary human UPS samples. Shades of red indicate significance by $-\log_{10} P$. **J,** Volcano plot representation of fold change in gene expression values (logFC) from RNA-seq in normal adult skeletal muscle versus UPS patient sample#1. **K,** GSEA of gene expression changes from human UPS sample #1 compared with normal human skeletal muscle tissue. Pathway analysis was performed with genes passing differential expression analysis [false discovery rate (FDR) < 0.25] and preranked by logFC.

Downloaded from http://aacrjournals.org/cancerres/article-pdf/78/10/2705/2764759/2705.pdf by guest on 27 August 2022

confirmed that genes of the "TNFA signaling via NFκB" pathway are significantly and increasingly differentially expressed in UPS compared with skeletal muscle (Fig. 2K), whereas "myogenesis" associated gene expression is inhibited in these tumors (Supplementary Fig. S2F). These RNA-Seq observations validate the utility of the H3K27Ac ChIP-Seq predicting the transcriptional profile of UPS. Thus, we have identified a "pro-proliferation" gene signature in human UPS that correlates well with our observations in the KP GEMM.

NFκB activity promotes UPS sarcomagenesis

The ChIP-seq and RNA-seq experiments described above were performed on a limited number of fresh frozen patient samples ($n = 3$) due to the paucity of available UPS tissues. Therefore, we sought a larger scale approach to evaluate NFκB activity in human UPS tissues. We performed IHC of 20 independent human skeletal muscle UPS tumor sections provided by Dr. Kumarasen Cooper (Department of Pathology & Lab Medicine, University of Pennsylvania, Philadelphia, PA). We evaluated active NF-κB (phospho-p65/p-p65) and YAP1 protein levels and found that both proteins are highly expressed in approximately 80% of tumors (Fig. 3A) relative to normal adjacent muscle tissue (Fig. 3B–D) and the expression is specifically nuclear. To confirm the functional importance of NFκB signaling in UPS, we inhibited *Rela* (the gene encoding p65) with two independent and specific shRNAs in KP cells. *Rela* shRNA #1 reduced expression by approximately 50%. shRNA #2 was less effective, reducing expression by only approximately 25% (Fig. 3E and F). Control and *Rela* shRNA–expressing KP cells were implanted subcutaneously into nude mice. Importantly, Loss of *Rela* significantly reduced final tumor volume (Fig. 3G and H) and weight (Fig. 3I) and these reductions directly correlated with the degree of knockdown provided by each shRNA. On the basis of these findings, we postulated that sarcoma cells are sensitive to NFκB inhibitors. We compared proliferation of KP cells treated with two independent NFκB inhibitors caffeic acid phenethyl ester (CAPE; refs. 33, 34) and BAY 11-7085 (35) to similarly treated HCT-116 colorectal cancer cells. HCT-116 cells are thought to be particularly sensitive to NFκB inhibition (36). KP cells are two times as sensitive to CAPE inhibition and three times as sensitive to BAY 11-7085 as HCT-116 cells (Fig. 3J and K). Together, these findings clearly show that NFκB activity promotes UPS growth and that YAP1 expression correlates with NFκB upregulation in human UPS.

Dual epigenetic therapy inhibits YAP1-mediated sarcoma proliferation

On the basis of our identification of YAP1 as a mediator of tumorigenesis, we sought inhibitory small-molecule approaches *in vivo*. The existing YAP1 inhibitor (i.e., verteporfin) has nonspecific effects as well as cell permeability challenges. Recent findings from our group and others suggest a strong epigenetic basis for soft tissue sarcoma development and efficacy of HDAC inhibitors in preclinical UPS models (18, 37–39). Similarly, Mazur and colleagues published an RNA-seq dataset of KP-driven PDAC that suggested epigenetic modulation increased expression of the key YAP1 inhibitor *AMOT* (40). Therefore, we queried whether inhibitors of chromatin modifiers/readers would be effective against muscle-derived UPS in a YAP1-dependent manner. We hypothesized that the chromatin landscape in UPS is permissive with regard to NFκB signaling, which promotes constitutive activation of NFκB SEs. Therefore, we focused on inhibitors that modify the SE landscape, such as the bromodomain inhibitor, JQ1 (41). To test this hypothesis, we initially treated three independent sarcoma cell lines with increasing doses of JQ1, including human fibrosarcoma cells, KP cells, and a cell line derived from a second sarcoma muscle UPS GEMM, the KIA model. Although not specifically a muscle-derived tumor, some fibrosarcomas are now thought to be genetically indistinguishable from UPS (2). Consistent with this observation, HT-1080 fibrosarcoma cells require YAP1 for proliferation and share critical proliferation mechanisms with UPS cells (7). Therefore, we included HT-1080 cells in our current studies. All three cell lines were sensitive to JQ1 (Supplementary Fig. S3A). Therefore, we tested the effect of 50 mg/kg daily JQ1 on our KP-derived subcutaneous allograft sarcoma model in nude mice. JQ1 dramatically reduced tumor progression (Fig. 4A) with a 5-fold reduction in final tumor volume (Fig. 4B) and a 6-fold reduction in final tumor weight (Fig. 4C) compared with DMSO-treated controls. Interestingly, we also found that JQ1 inhibits expression of Yap1 *in vivo* (Fig. 4D; Supplementary Fig. S3B). Given JQ1's many potential molecular effects, a rescue assay was performed to determine whether JQ1-mediated inhibition of proliferation is YAP1-dependent. We used HT-1080 cells, which are sensitive to 250 nmol/L JQ1, easily transduced, and proliferate under control conditions at a less rapid pace than the other sarcoma cell lines. This last parameter is important because it allowed us to ectopically express a constitutively nuclear/active YAP1 mutant, YAP1(S6A), and observe the expected significant increase in proliferation (Fig. 4E), a necessary positive control for the rest of the experiment. YAP1(S6A) rescued approximately 40% of the JQ1-induced proliferation deficit by day 5 (Fig. 4E). To confirm that the role of YAP1 in proliferation is dependent on its nuclear functions, we performed a similar rescue assay using WT-YAP1, which is shuttled back and forth from the nucleus to the cytoplasm. WT-YAP1 also rescued proliferation, but the effects were less substantial as predicted (Fig. 4F). Similar, but less dramatic results were observed in the more proliferative KP cells (Supplementary Fig. S3C). Western blot analysis of mutant and WT YAP1–expressing cells shows the level of expression of V5-tagged constructs in each condition (Supplementary Fig. S3D). Consistent with the above findings, we observed that 250–500 nmol/L JQ1 treatment lowers *YAP1* mRNA levels by 50% in HT-1080, KIA, and KP cells (Supplementary Fig. S3E and S3F).

In some cancer contexts, the efficacy of JQ1 is dependent on its ability to inhibit the *MYC* oncogene. However, that is not the case in the sarcoma subtypes we studied (Supplementary Fig. S4A–S4D). Our previously published work showed that the pan-HDAC inhibitor SAHA suppressed sarcoma proliferation *in vitro* and tumor growth *in vivo* by 50% (18) and we hypothesized that combination SAHA/JQ1 treatment would be more effective than either drug individually. MTT proliferation studies comparing dose escalation of SAHA and JQ1 separately and in combination showed that the combination of both drugs at lower doses is more effective than either drug alone *in vitro* (Fig. 4G and H; Supplementary Fig. S4E). Consistent with our proliferation findings, combination therapy [SAHA (2 μmol/L)/JQ1 (0.5 μmol/L)] most effectively inhibited expression of both Yap1 and its transcriptional target Foxm1 in KP cells (Fig. 4I). We saw similar effects on YAP1 and FOXM1 in six additional human sarcoma cell lines representing

Downloaded from http://aacrjournals.org/cancerres/article-pdf/78/10/2705/2764759/2705.pdf by guest on 27 August 2022

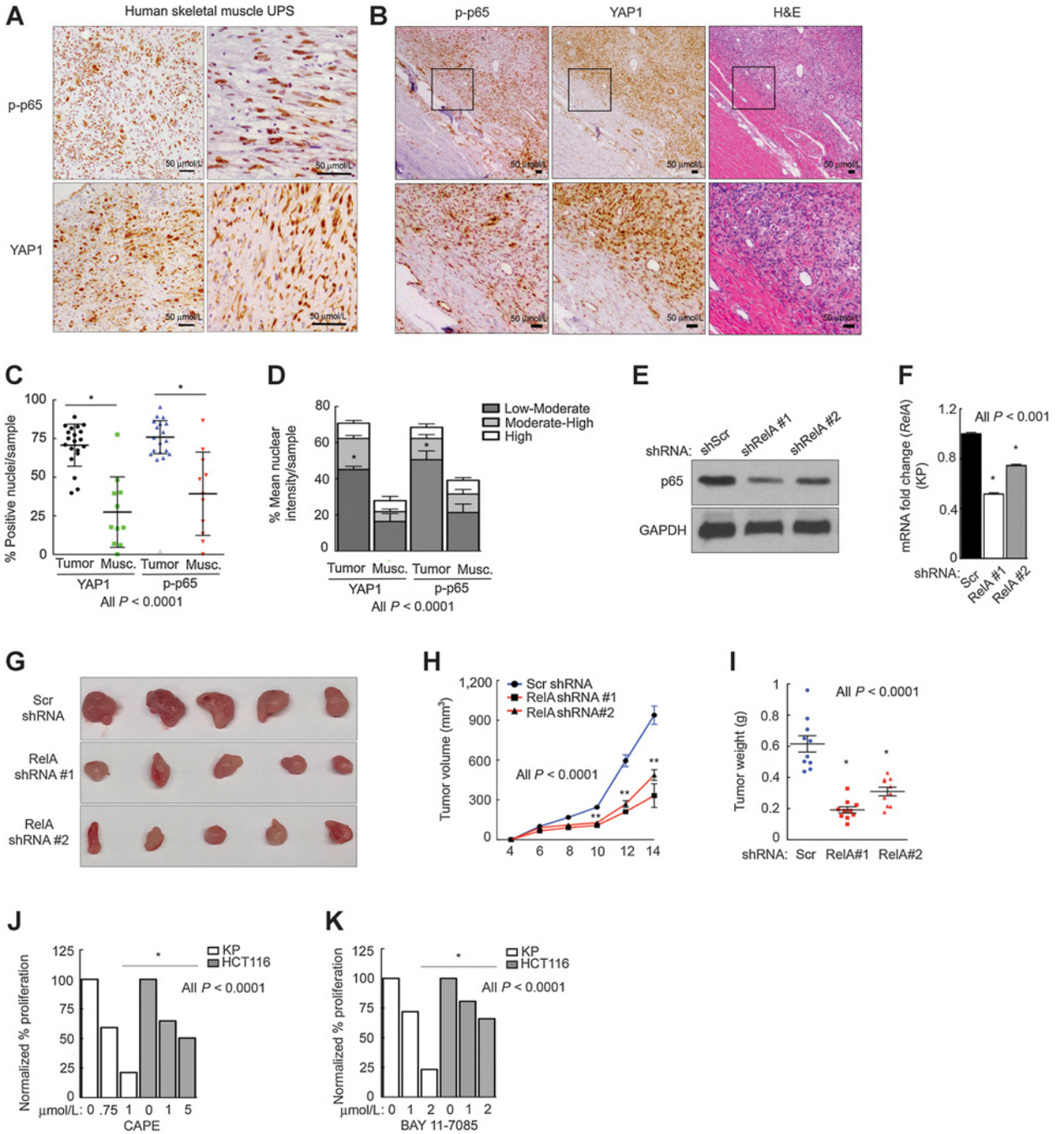

Figure 3.

NFκB activity is upregulated in human UPS. **A** and **B,** IHC of UPS tumors. IHC of UPS tumor sections at the invading edge of normal adjacent muscle. Scale bar, 50 µm; $n = 20$. **C,** Twenty tumor sections were quantified. **D,** Positive nuclei were stratified into low-moderate, moderate-high, and high expression for YAP1 and p-P65. Western blot analysis (**E**) and qRT-PCR (**F**) of KP cells expressing shRNAs targeting p65/*RelA* (NF-κB). **G,** Images of subcutaneous KP tumors. Tumor volume (**H**) and weights (**I**) from shRNA-expressing KP tumors. KP and HCT116 cell proliferation after treatment with CAPE (**J**) and BAY 11-7085 (**K**) for 72 hours; SD. H&E, hematoxylin and eosin.

multiple subtypes including rhabdomyosarcoma, liposarcoma, leiomyosarcoma, and UPS (Supplementary Fig. S4F). These findings suggest potential broader applicability of SAHA/JQ1 against human sarcomas.

We sought to determine how SAHA/JQ1 inhibits YAP1 activity so effectively. In addition to AMOT-mediated inhibition of YAP1, its activity is regulated by Hippo kinase LATS1/2-dependent phosphorylation (42). SAHA/JQ1 treatment does not change

Downloaded from http://aacrjournals.org/cancerres/article-pdf/78/10/2705/2764759/2705.pdf by guest on 27 August 2022

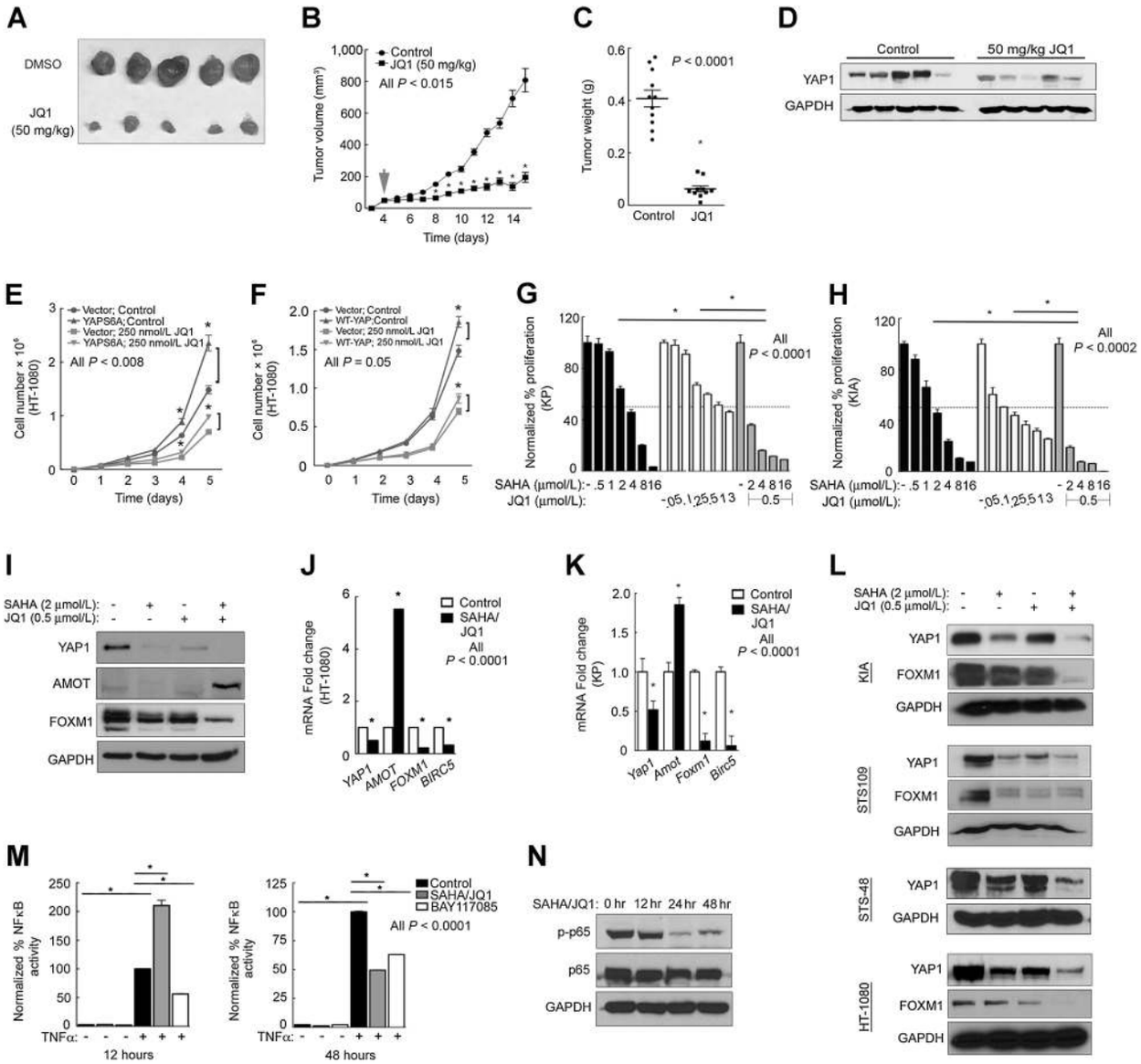

Figure 4.

Epigenetic modulation by SAHA/JQ1 inhibits sarcoma growth *in vivo*. **A,** Representative tumors from DMSO- ($n = 10$) and JQ1- (50 mg/kg per day; $n = 10$) treated mice. Tumor volume (**B**) and weight (**C**) from DMSO and JQ1 cohorts; SEM. Arrow, beginning of treatment at tumor volume = 100 mm^3. **D,** Western blots of DMSO- and JQ1-treated tumors. Proliferation assay of HT-1080 cells expressing mutant YAPS6A (**E**) or WT-YAP (**F**) with or without 250 nmol/L JQ1; SEM. Seventy-hour MTT proliferation assay of KP (**G**) and KIA (**H**) cells treated with SAHA/JQ1; SEM. **I,** Western blot analysis of KP cells treated with SAHA (2 μmol/L), JQ1 (0.5 μmol/L), or both for 48 hours. qRT-PCR of HT-1080 (**J**) and KP (**K**) cells treated as in **I**; SEM. **L,** Western blots of HT1080, KIA, STS-48, and STS-109 cells treated as in **I**. **M,** NFκB luciferase reporter assay performed in KP cells treated with SAHA (2 μmol/L)/JQ1 (0.5 μmol/L) and BAY11-7085 for 12 or 48 hours. Twenty hours prior to detection of luciferase activity, we treated with PBS or TNFα (10 ng/mL); SEM. **N,** Western blots of KP cells.

expression of the upstream hippo kinases MST1/2 or LATS1 (Supplementary Fig. S4G and S4H). However, we did observe a modest increase in LATS1 phosphorylation, suggesting a possible but likely minor increase in activity (Supplementary Fig. S4G*). Importantly, YAP1 phosphorylation and cytoplasmic localization increased substantially in response to SAHA/JQ1 (Supplementary Fig. S5A and S5B). Therefore, we focused on AMOT-mediated YAP1 inhibition.

Importantly, *AMOT* is highly expressed in human skeletal muscle (43, 44), but is lost in all commonly diagnosed sarcomas according to the Detwiller and colleagues' sarcoma dataset (Supplementary Fig. S6A; ref. 45). Our RNA-seq of human UPS confirmed this finding (Fig. 2J), suggesting that AMOT may function as a tumor suppressor in sarcoma. To test whether Amot is the predominant inhibitor of Yap1 in our cells, we used the Tankyrase inhibitor XAV939, which stabilizes Amot protein levels (46). Increasing doses of XAV939 clearly result in higher levels of YAP1 phosphorylation and loss of total YAP1 (Supplementary Fig. S6B). To confirm that expression of AMOT suppresses proliferation in sarcoma, we transduced human HT-1080 cells with

Downloaded from http://aacrjournals.org/cancerres/article-pdf/78/10/2705/2764759/2705.pdf by guest on 27 August 2022

GFP-tagged WT-AMOT. We sorted the GFP-AMOT$^+$ population to 85% purity (Supplementary Fig. S6C). By immunofluorescence (IF), we observed that GFP-AMOT appropriately localizes to the perinuclear region as has been previously reported (Supplementary Fig. S6D; ref. 47). Control vector and GFP-AMOT expressing cells were pulsed with fluorescent CellTrace dye. CellTrace levels were appropriately depleted during each control cell division as dye molecules are distributed to daughter cells. GFP-AMOT–expressing cells quantified by flow cytometry contained approximately 50% more CellTrace than control cells, indicating that cell division in experimental cells was reduced by half (Supplementary Fig. S6E). Furthermore, analysis of the control GFP$^+$ and GFP-AMOT$^+$ cells at day 5 revealed that AMOT-GFP$^+$ cells only are reduced from approximately 85% to approximately 45% of the population, having been overtaken in culture by GFP$^-$ cells (Supplementary Fig. S6F). Our findings show that expression of AMOT is a strong YAP1 inhibitor in our cells and accordingly suppresses sarcoma cell proliferation.

Together, our studies revealed an AMOT-dependent mechanism of YAP1 degradation in SAHA/JQ1–treated sarcoma cells. Consistent with this observation, loss of *YAP1* transcription, together with increased expression of *AMOT*, resulted in near ablation of YAP1 targets *FOXM1* and *BIRC5* in SAHA/JQ1–treated cells (Fig. 4I–K). We expanded our observations to include additional murine (KIA) and human (STS-48, STS-109) UPS cell lines (Fig. 4L). Next we asked whether SAHA/JQ1 treatment altered NFκB signaling. Using the NFκB luciferase system in KP cells, we evaluated NFκB activity after 12 or 48 hours of SAHA/JQ1 treatment. The NFκB inhibitor BAY 11-7085 was used as a control and reduced NFκB activity by 50% at both time points. We observed that NFκB activity doubled after 12 hours of SAHA/JQ1 treatment and then plummeted to 50% of the TNFα-treated positive control at 48 hours (Fig. 4M). This finding is consistent with published observations that NFκB transcriptional activity is extremely dynamic and oscillates over time in response to stimuli (48). However, we observed that phosphorylation of p65, a key readout of NFκB activity, remains high after 12 hours of SAHA/JQ1 treatment (Fig. 4N). We hypothesize that elevated NFκB activity after 12 hours of treatment is due to increased nuclear localization of p-p65. By 48 hours of treatment, p-p65 levels were substantially reduced. These observations suggest that SAHA/JQ1 may induce oscillation, but that treatment ultimately reduces NFκB signaling.

SAHA/JQ1 mediates loss of YAP1 and induces a differentiated muscle transcriptional program

Combination SAHA/JQ1 treatment inhibits Yap1 and dramatically reduces proliferation of sarcoma cells (Fig. 4G–I). One possible explanation for this finding is induction of apoptosis or differentiation. Importantly, persistent YAP1 and NFκB signaling are central components of myoblast proliferation and are suppressed during differentiation (14, 16, 49–51). Therefore, we tested the possibility that epigenetic therapy differentiates sarcoma cells into a less malignant muscle-like cell. First, we evaluated NFκB signaling in the C2C12 murine model of normal myoblast differentiation. We treated undifferentiated C2C12 myoblasts with differentiation media (DM) for up to 6 days and evaluated differentiation markers, NFκB targets, and myotube formation. Differentiation markers (*Myh1*, *Myh2*, *Mef2c*, and *Myh3*) were all upregulated dramatically by day 6 (Fig. 5A), coincident with myotube formation (Fig. 5B). We also observed that expression of the YAP1-dependent NFκB targets *Ccl2* and *Hbegf* oscillated over time (Fig. 5C), consistent with our NFκB luciferase activity observations (Fig. 4M) and published findings (48). Furthermore, YAP1-mediated NFκB targets/regulators (*Ccl2*, *Hbegf*, *Areg, and Phlda1*) did not oscillate in proliferating C2C12 cells in growth media (GM) for 3 days (Fig. 5D). Beyond 3 days, confluence initiates expression of differentiation markers, and we can no longer accurately measure proliferation-associated gene expression. We next evaluated expression of these targets in KP cells treated with SAHA/JQ1 and observed the oscillation associated with myoblast differentiation (Fig. 5E). Interestingly, NFκB targets do not oscillate synchronously either in SAHA/JQ1–treated KP cells or in differentiating C2C12 cells (Fig. 5C), suggesting that timing of target expression may be dependent on production of specific NFκB cofactors (52). The temporal oscillation of individual targets will have to be studied in depth to fully understand the role of these patterns in differentiation and proliferation. Our data suggest that epigenetic therapy of sarcoma cells restores the NFκB oscillation observed in differentiating myoblasts. Consistent with this hypothesis, SAHA/JQ1–treated KP cells have a significantly different morphology than control or individually drug-treated cells, although they do not form myotubes, many cells appear flat, multinucleated, and in some cases seem to be merging (Fig. 5F, arrows). To determine whether a muscle differentiation program is induced transcriptionally, we analyzed differential changes in gene expression by microarray of DMSO and SAHA/JQ1–treated KP cells. Metascape analysis of genes enriched in DMSO-treated cells showed most significant association with cell cycle and cell division (Fig. 5G). However, genes enriched in SAHA/JQ1–treated cells were associated with numerous processes linked to normal muscle function, including endoplasmic reticulum (ER) stress, autophagy, catabolic metabolism, mitochondrial function, and lipid processing (Fig. 5H). (53). Similarly, Ingenuity Pathway Analysis (IPA) of our KP/KPY tumor microarray revealed that Yap1 loss induces ER stress and unfolded protein response (UPR), as well as the expected changes in TNF receptor signaling suggesting that YAP1 contributes specifically to these processes during muscle differentiation (Supplementary Fig. S7A). The lack of induction of pathways associated with terminal skeletal muscle differentiation including hallmark "Myogenesis" suggests that SAHA/JQ1 promotes incomplete differentiation. To validate upregulation of a muscle phenotype in SAHA/JQ1–treated cells, we evaluated expression of the muscle differentiation markers *MEF2C, MYOD1, and CDKN1C* (p57). Both *MEF2C* and *CDKN1C* mRNA levels were substantially increased due to SAHA/JQ1 treatment in KP and HT-1080 cells (Fig. 5I and J). However, *MYOD1* mRNA levels were unaffected (Fig. 5I). MYOD is regulated at the protein level by its physical interaction with p57 (54); therefore, we tested expression of Myod and p57 by Western blotting of murine (Fig. 5K) and human (Fig. 5L) UPS cells and saw both proteins were increased in drug-treated cells. Importantly, expression of YAP1 and its transcriptional target FOXM1 (7) were nearly abolished (Fig. 4I–L). We saw similar effects in HT-1080 cells. Together, these findings show that combination SAHA/JQ1 treatment promotes differentiation, potentially due to inhibition of YAP1-mediated transcriptional regulation.

YAP1 promotes NFκB signaling by suppressing USP31 expression

Next we sought to determine whether Yap1 inhibition via SAHA/JQ1 mediates the differentiation phenotype and identify the

Downloaded from http://aacrjournals.org/cancerres/article-pdf/78/10/2705/2764759/2705.pdf by guest on 27 August 2022

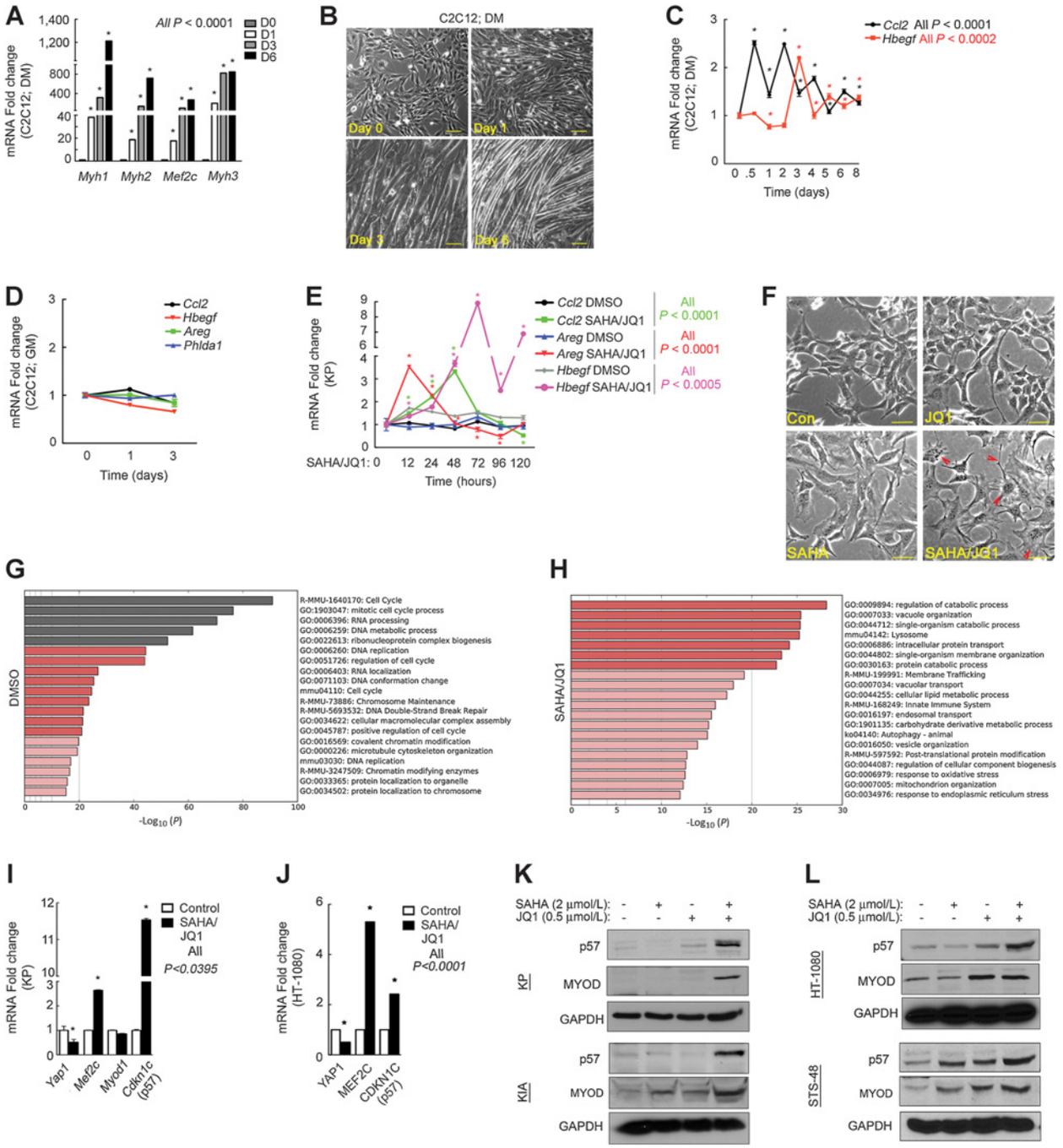

Figure 5.

SAHA/JQ1 decreases sarcomagenesis by inducing muscle differentiation. **A,** qRT-PCR of C2C12 cells treated with differentiation media (DM) for 0, 1, 3, or 6 days; SD (days 1, 3, and 6 are compared with day 0 for each target). **B,** Images of C2C12 cells forming myotubes. Scale bars, 50 μm. **C,** qRT-PCR of C2C12 cells treated as in **A**; SD. **D,** qRT-PCR of C2C12 cells treated with growth media (GM); SD. **E,** qRT-PCR of KP. (SAHA/JQ1) were compared with control-treated cells at each time point; SD. **F,** Images of KP cells treated as in **D**. Scale bars, 100 μm. Pathway enrichment analysis (via Metascape) of genes identified by microarray and enriched in KP cells treated with DMSO (**G**) or SAHA/JQ1 (**H**) for 48 hours. Shades of red indicate significance by −log10 *P*. qRT-PCR of KP (**I**) and HT-1080 (**J**) cells treated as in **D**; SEM. Western blot analysis of murine (KP, KIA; **K**) and human (HT1080 and STS-48; **L**) sarcoma cells treated as in **D**.

associated mechanism. First, we investigated whether SAHA (2 μmol/L)/JQ1 (0.5 μmol/L) treatment induced apoptosis. We performed Annexin V/Propidium Iodide (PI) assays by flow cytometry using 1 μmol/L staurosporin as a positive control. Whereas staurosporin treatment dramatically increased Annexin/PI positivity compared with vehicle control, SAHA/JQ1 did not alter apoptotic

Downloaded from http://aacrjournals.org/cancerres/article-pdf/78/10/2705/2764759/2705.pdf by guest on 27 August 2022

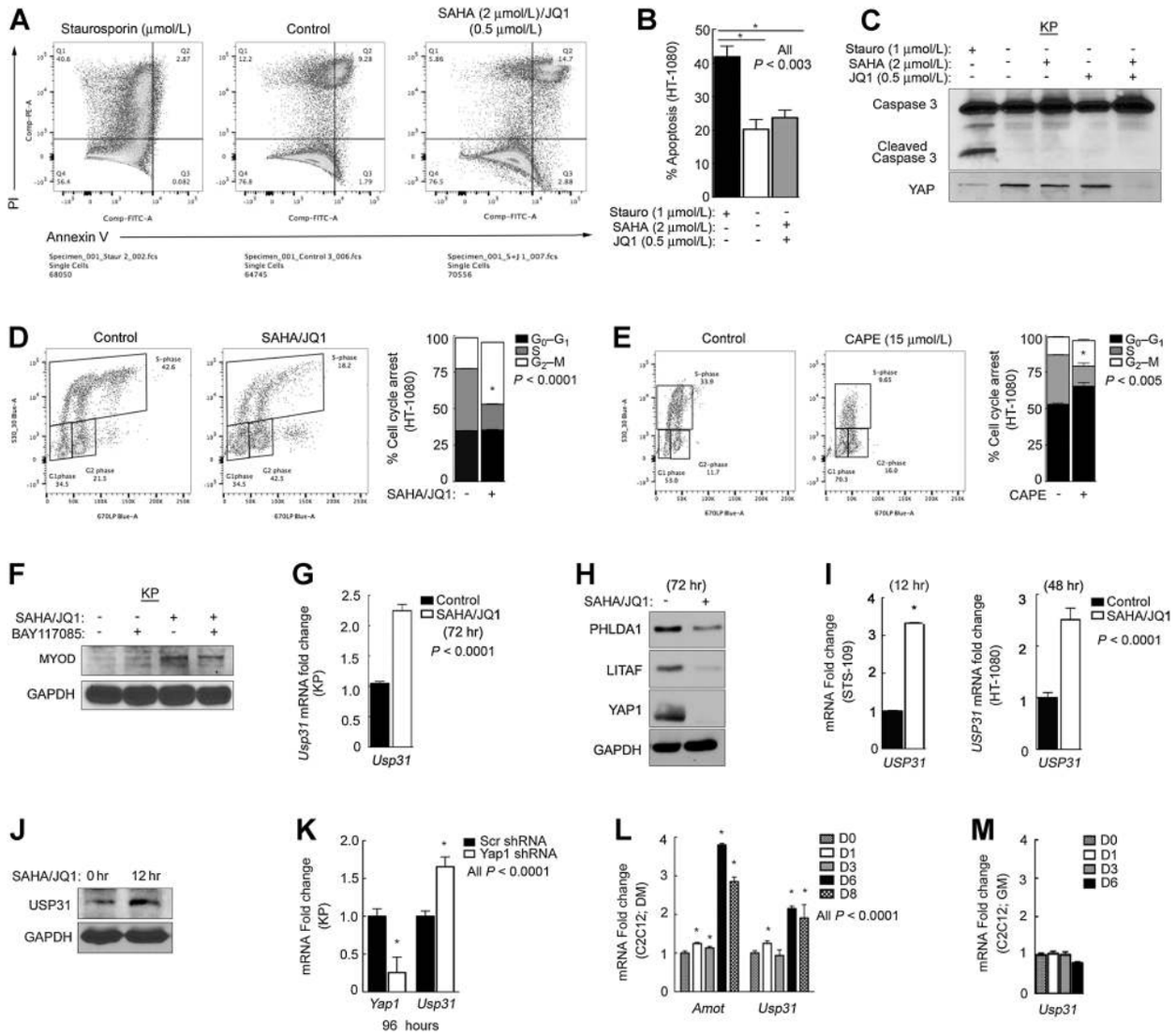

Figure 6.

YAP1 regulates NFκB signaling pathway through USP31. Representative flow cytometry plots (**A**) and quantification of percentage of Annexin V/PI–positive HT-1080 cells (**B**) treated with SAHA (2 μmol/L)/JQ1 (0.5 μmol/L) for 48 hours. Six hours prior to harvest, positive control cells were treated with 1 μmol/L staurosporin to induce apoptosis; SEM. **C,** Western blot analysis of KP cells treated as in **A**. **D,** Representative flow cytometry plots and quantitation of BrdUrd incorporation in HT-1080 cells treated as in **A**. **E,** Representative flow cytometry plots and quantitation of BrdUrd incorporation in HT-1080 cells treated with CAPE (15 μmol/L) for 48 hours. **F,** Western blots of SAHA/JQ1 (2 μmol/L)/(0.5 μmol/L)- and BAY 11-7085 (1.5 μmol/L)-treated KP cells. **G,** qRT-PCR of KP cells treated as in **A**; SD. **H,** Western blot analysis of KP cells treated as in **A**. **I,** qRT-PCR of human UPS (STS-109) and HT-1080 cells as in **A**; SD. **J,** Western blot analysis of STS-109 cells treated as in **A**. **K,** qRT-PCR of KP cells expressing *Yap1*-specific shRNA for 96 hours. **L,** qRT-PCR of C2C12 cells treated with differentiation media for 0–8 days; SD. **M,** qRT-PCR of C2C12 cells treated with growth media (GM) for 0–8 days.

levels (Fig. 6A and B). Consistent with these findings, we observed no change in cleaved caspase-3 levels due to SAHA/JQ1 treatment, whereas staurosporin induced the predicted increase in caspase-3 cleavage (Fig. 6C; Supplementary Fig. S7B). Next, we tested the prediction that dampening NFκB signaling recapitulates the effect of SAHA/JQ1 on the cell cycle. We treated sarcoma cells with the NFκB inhibitor CAPE and performed bromodeoxyuridine (BrdUrd) analysis by flow cytometry and compared the results with SAHA/JQ1–treated cells. Both treatments induced cell-cycle arrest in G_2 phase, although SAHA/JQ1 is significantly more effective (Fig. 6D and E). To determine whether NFκB inhibition alone is sufficient to induce Myod expression and differentiation, we investigated Myod levels in sarcoma cells treated with the NFκB inhibitor BAY117085 and found that NFκB inhibition alone could not induce MYOD1 protein expression (Fig. 6F). Additional epigenetic changes due SAHA/JQ1 are necessary to facilitate the muscle differentiation program.

Given the widespread effects of YAP1 signaling on NFκB activity (Fig. 1I–K and M), we hypothesized that a critical upstream regulator of the NFκB pathway is modulated by YAP1.

Downloaded from http://aacrjournals.org/cancerres/article-pdf/78/10/2705/2764759/2705.pdf by guest on 27 August 2022

Recently identified as a critical upstream negative regulator of NFκB, the peptidase USP31 controls ubiquitination of the TRAF molecules, which convey signals initiated by TNFα receptor engagement downstream to p65/NFκB (19). *Usp31* levels increase in response to SAHA/JQ1 in murine KP cells (Fig. 6G). Interestingly, the time point at which *USP31* induction is maximal varies between cell lines according to rate of proliferation. Rapidly growing KP cells require 72 hours of treatment. Consistent with this observation, 72 hours of drug treatment in KP cells decreased expression of NFκB targets we identified as upregulated in human UPS (Fig. 2A, *Litaf*) and as Yap1-mediated in KP tumors (Fig. 1I and K, *Phlda1*; Fig. 6H). The importance of this observation will be defined in later studies. Slower growing human fibrosarcoma (HT-1080) and UPS (STS-109) cells only need 12–48 hours to induce maximal USP31 (Fig. 6I and J). Importantly, these findings support the conclusion that SAHA/JQ1 inhibits NFκB activity in multiple cell lines and sarcoma subtypes. Furthermore, genetic inhibition of *Yap1* via specific shRNA also induces *Usp31* expression, indicating that this phenotype is mediated by YAP1 (Fig. 6K). To ascertain the relevance of Usp31 expression in muscle cell differentiation, we evaluated differentiating C2C12 cells and observed that *Usp31* expression increases during the 8-day course of differentiation (Fig. 6L). *Amot* levels increase during precisely the same time period in C2C12 cells, indicating that loss of Yap1 activity occurs simultaneously with induction of *Usp31*. Importantly, *Usp31* levels remained consistent in proliferating C2C12 cells (Fig. 6M). Together, these findings support the hypothesis that YAP1 suppresses USP31 and in doing so maintains persistently high levels of NFκB activity, signaling, and proliferation.

USP31 mediates effects of SAHA/JQ1 and YAP1 loss on NFκB activity and tumorigenesis

To determine the functional outcome of *Usp31* expression, we silenced it with specific shRNA. Fifty percent loss of *Usp31* expression significantly increased *in vitro* KP cell proliferation (Fig. 7A). These data are consistent with increased NFκB activity. Moreover, in the luciferase reporter system *Usp31* shRNA expression rescued SAHA/JQ1–mediated suppression of NFκB activity. This finding clearly shows that Usp31 mediates the effects of SAHA/JQ1 on NFκB activity (Fig. 7B). To confirm that drug treatment inhibits NFκB signaling through upregulation of Usp31 we evaluated the early NFκB regulator and direct target of Usp31 peptidase activity, Traf2. K63 linked ubiquitination of Traf2 is dependent upon Usp31 (19). Interestingly, Traf2 protein expression is lost in SAHA/JQ1–treated cells (Fig. 7C, top), whereas our microarray analysis of KP cells showed that *Traf2* mRNA levels were not significantly altered relative to *Yap1* and its transcription targets *Foxm1* and *Birc5* (Fig. 7C, bottom). These data suggest that Usp31-mediated K63-linked ubiquitination affects Traf2 protein stability. However, this hypothesis and the nature of YAP1-mediated suppression of USP31 expression (direct vs. indirect) require additional investigation. To show that Yap1's effect on proliferation is predominantly due to its control of Usp31 expression, we performed an *in vivo* rescue allograft assay. KP cells were infected with control or *Yap1* shRNA–expressing lentivirus, puromycin selected for 48 hours, then infected with control or *Usp31* shRNA lentivirus. Western blot analysis of Yap1 and qRT-PCR expression of *Usp31* confirms inhibition of expression in the appropriate cells (Fig. 7D). As we have previously reported, expression of *Yap1* shRNA significantly reduced tumor growth and weight compared with Scr shRNA control (7). Consistent with our *in vitro* proliferation findings (Fig. 7A), *Usp31*-specific shRNA increased tumor growth (Fig. 7E and F). Most importantly, loss of *Usp31* expression rescued the *Yap1* shRNA-mediated reduction in tumor growth. We therefore conclude that Usp31 suppression is critical for YAP1-dependent tumorigenesis.

SAHA/JQ1 inhibits sarcomagenesis in the KP model of UPS

One of our major goals is to identify novel therapeutic approaches for the treatment of UPS and other sarcomas. To test the potential efficacy of SAHA/JQ1 as a therapeutic strategy, we tested effects of the drug combination *in vivo* in KP GEMM tumors using 25 mg/kg SAHA and 50 mg/kg JQ1 (Fig. 7G). These doses and the precise schedule were optimized in detail due to the loss of several animals in pilot experiments from drug toxicity. The schedule presented here was safe and no animals died from drug administration. SAHA/JQ1 treatment caused statistically significant tumor regression in this very aggressive autochthonous model (Fig. 7H). Furthermore, the combined therapy delayed time to maximum tumor volume by 2-fold (Fig. 7I). Median survival of animals bearing control-treated tumors was 19 days relative to 25 days (SAHA) and 33 days (JQ1). The combination of SAHA and JQ1 was most effective with a median survival of 39 days ($\chi^2 P < 0.0001$). Importantly, Amot levels were significantly elevated in SAHA/JQ1–treated KP tumor tissue compared with controls (Fig. 7J), which is consistent with our *in vitro* findings. Subsequent IHC of SAHA/JQ1–treated KP autochthonous tumors revealed that Myod levels were elevated while Ki67 positivity was lost *in vivo* (Fig. 7K). Together, these findings show that epigenetic modulation of the Hippo pathway restores normal NFκB activity, leads to decreased sarcomagenesis, and increased muscle differentiation *in vivo* via Usp31.

Discussion

Targetable oncogenic driver mutations are rare in sarcomas. As a result, there are no effective targeted therapies. Our goal was to identify mutant oncogene-independent mechanisms of sarcomagenesis in the subtypes common to adults (i.e., UPS and fibrosarcoma) and potential therapeutic interventions. Our study highlights the efficacy of combined epigenetic inhibitors against UPS. Although not specific inhibitors, SAHA and JQ1 may provide a new option for these patients.

In this study, we focused on understanding the pathways regulated by YAP1 in sarcomagenesis. Through genetic and epigenetic studies, we found that YAP1 contributes to hyperactivation of NFκB, a signaling pathway with a crucial role in muscle progenitor cell division and differentiation. In fact, ChIP-seq for H3K27Ac and super enhancer analysis of human UPS samples led to the identification of NFκB as the most transcriptionally active pathway in UPS. YAP1-mediated control of NFκB target expression was confirmed in a GEMM of sarcoma. On the basis of our findings, we postulate that NFκB signaling is consistently upregulated in human UPS and is enhanced by persistent YAP1 stabilization.

NFκB signaling is complex and requires the expression and posttranslational modification of multiple key effectors. Our studies revealed that YAP1 promotes NFκB activity by controlling expression and stability of several key upstream regulators of NFκB signaling (i.e., USP31 and TRAF2). Using our YAP1-deficient UPS GEMM, specific shRNAs, and SAHA/JQ1, we

Downloaded from http://aacrjournals.org/cancerres/article-pdf/78/10/2705/2764759/2705.pdf by guest on 27 August 2022

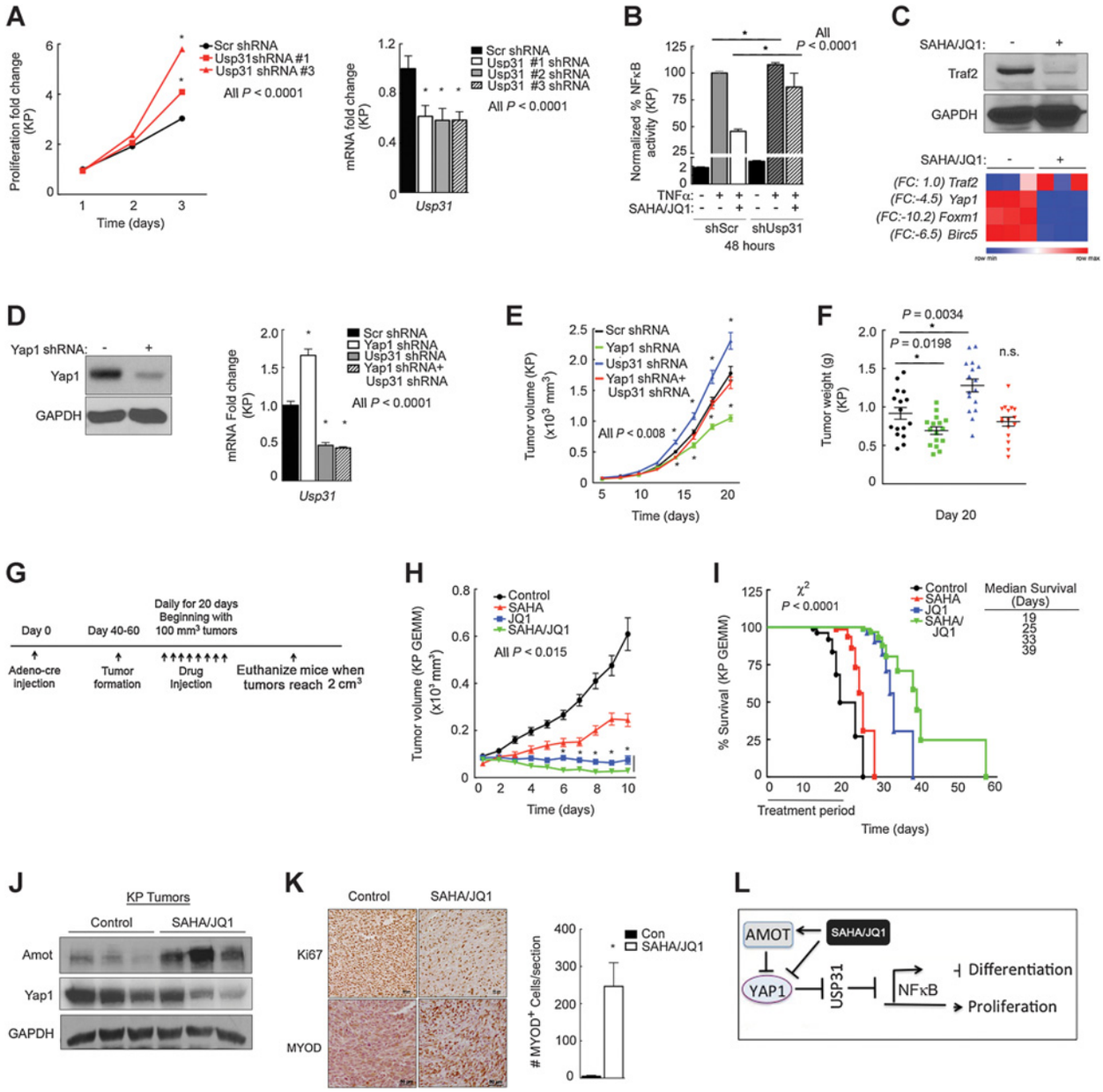

Figure 7.

Yap-mediated suppression of USP31 promotes proliferation and opposes differentiation. **A,** Left, proliferation assay of *Usp31* shRNA–expressing KP cells. Right, qRT-PCR of shRNA-treated cells; SD. **B,** NFκB luciferase reporter in KP cells. shSCR + TNFα versus shUsp31 + TNFα, DMSO + shSCR + TNFα versus SAHA/JQ1 + shUsp31 + TNFα; SD. **C,** Top, KIA cells treated with SAHA (2 μmol/L)/JQ1 (0.5 μmol/L) for 48 hours. Bottom, Broad Institute Morpheus analysis of microarray results from Fig. 5G and H. FC, fold change. *Q* values: *Traf2* (39.4), Yap1 (0), Foxm1 (0), Birc5 (0). **D,** Western blot analysis (left) and qRT-PCR (right) from KP cells prior to injection. Tumor volume (**E**) and tumor weights (**F**) from subcutaneous allografts of KP cells treated with lentivirus expressing shRNAs; SEM. **G,** Drug scheduling for KP GEMM beginning when tumors measured 100 mm^3. **H,** Initial 10-day tumor volumes of SAHA- and JQ1-treated KP tumors; SEM. **I,** Survival curve (endpoint, tumor volume of 2 cm^3) of drug-treated tumors ($n = 10$ mice per group from two cohorts). Log-rank χ^2. **J,** Western blot analysis of KP tumors harvested after 20 days of treatment. **K,** IHC for Ki67 and MYOD1. Scale bar, 50 μm. **L,** Model of proposed molecular mechanism.

determined that NFκB target expression, transcriptional activity, and phosphorylation/activation of p65 (the key dimer of the NFκB transcription factor) are all decreased when YAP1 is lost. Importantly, our studies reveal two parallel alterations in NFκB signaling found in human UPS (i) upregulation of YAP1 alters expression USP31, a negative regulator of NFκB and (ii) chromatin modification at NFκB target loci is modified to allow transcription of critical genes. Together, these conditions promote NFκB activity and sarcomagenesis.

Here we also report that the mechanism by which SAHA/JQ1 inhibits YAP1 expression is multi-pronged. The combination decreases YAP1 mRNA levels by ∼50% and increases expression

Downloaded from http://aacrjournals.org/cancerres/article-pdf/78/10/2705/2764759/2705.pdf by guest on 27 August 2022

of the YAP1 inhibitor, AMOT, which is silenced in UPS compared to normal skeletal. SAHA/JQ1 restores AMOT expression, inhibiting YAP1 activity. SAHA/JQ1 treatment restores control of Hippo pathway signaling, inhibiting proliferation and simultaneously initiating a muscle differentiation transcriptional program.

The most critical YAP1 target we identified was the novel ubiquitin peptidase USP31. Virtually nothing is known about USP31 beyond its structure and connection to NFκB signaling (19, 55). USP31 was induced in response to YAP1 inhibition and SAHA/JQ1. Importantly, we observed that *Usp31 was* upregulated in differentiating C2C12 myoblasts, suggesting that in sarcoma cells SAHA/JQ1 and Yap1 loss may restore differentiation (Fig. 7L). Together, our findings suggest that muscle-derived UPS cells behave like proliferating myoblasts incapable of undergoing differentiation due to persistent YAP1 and NFκB signaling. SAHA/JQ1 inhibits YAP1 and restores NFκB to patterns observed in differentiating myoblasts, forcing tumor cells to differentiate.

Overall, our work establishes NFκB, a key regulator of normal muscle development, as a pathway that becomes persistently upregulated during sarcomagenesis at least in part through aberrant suppression of the YAP1 target USP31. Collectively, our data suggest that YAP1 stabilization, p65 phosphorylation and *AMOT* suppression could potentially serve as useful biomarkers for UPS and provide the mechanistic rationale for epigenetic therapy to restore Hippo pathway activity to normal levels in the treatment of this disease.

Disclosure of Potential Conflicts of Interest

No potential conflicts of interest were disclosed.

Authors' Contributions

Conception and design: S. Ye, J. Qi, T.S.K. Eisinger-Mathason
Development of methodology: A. Rivera-Reyes, J. Qi
Acquisition of data (provided animals, acquired and managed patients, provided facilities, etc.): S. Ye, M.A. Lawlor, S. Egolf, S. Chor, K. Pak, G.E. Ciotti, A.C. Lee, G.E. Marino, J. Shah, D. Niedzwicki, P.M.C. Park, M.Z. Alam, M. Haldar, J. Qi
Analysis and interpretation of data (e.g., statistical analysis, biostatistics, computational analysis): S. Ye, M.A. Lawlor, A. Rivera-Reyes, P.M.C. Park, M. Xu, J. Qi, T.S.K. Eisinger-Mathason
Writing, review, and/or revision of the manuscript: S. Ye, K. Weber, A. Grazioli, J.A. Perry, J. Qi, T.S.K. Eisinger-Mathason
Administrative, technical, or material support (i.e., reporting or organizing data, constructing databases): J. Qi, T.S.K. Eisinger-Mathason
Study supervision: J. Qi, T.S.K. Eisinger-Mathason

Acknowledgments

We would like to thank John Tobias for assistance with bioinformatics, Fernando Camargo for providing the *Yap*$^{fl/fl}$ mice, and Kumarasen Cooper M.D., and Paul Zhang M.D. for their assistance with human tumor pathology. This work was funded by The University of Pennsylvania Abramson Cancer Center (to T.S.K. Eisinger-Mathason), The Penn Sarcoma Program Center (to T.S.K. Eisinger-Mathason), Steps to Cure Sarcoma Center (to T.S.K. Eisinger-Mathason), and NIH/NCI P50 CA100707 (to J. Qi).

The costs of publication of this article were defrayed in part by the payment of page charges. This article must therefore be hereby marked *advertisement* in accordance with 18 U.S.C. Section 1734 solely to indicate this fact.

Received December 29, 2017; revised February 1, 2018; accepted February 22, 2018; published first February 28, 2018.

References

1. Taylor BS, Barretina J, Maki RG, Antonescu CR, Singer S, Ladanyi M. Advances in sarcoma genomics and new therapeutic targets. Nat Rev Cancer 2011;11:541–57.
2. The Cancer Genome Atlas Research Network. Comprehensive and integrated genomic characterization of adult soft tissue sarcomas. Cell 2017; 171:950–65.
3. Lim J, Poulin NM, Nielsen TO. New strategies in sarcoma: linking genomic and immunotherapy approaches to molecular subtype. Clin Cancer Res 2015;21:4753–9.
4. Ballinger ML, Goode DL, Ray-Coquard I, James PA, Mitchell G, Niedermayr E, et al. Monogenic and polygenic determinants of sarcoma risk: an international genetic study. Lancet Oncol 2016;17:1261–71.
5. Pappo AS, Vassal G, Crowley JJ, Bolejack V, Hogendoorn PC, Chugh R, et al. A phase 2 trial of R1507, a monoclonal antibody to the insulin-like growth factor-1 receptor (IGF-1R), in patients with recurrent or refractory rhabdomyosarcoma, osteosarcoma, synovial sarcoma, and other soft tissue sarcomas: results of a Sarcoma Alliance for Research Through Collaboration Study. Cancer 2014;120:2448–56.
6. Wagner LM, Fouladi M, Ahmed A, Krailo MD, Weigel B, DuBois SG, et al. Phase II study of cixutumumab in combination with temsirolimus in pediatric patients and young adults with recurrent or refractory sarcoma: a report from the Children's Oncology Group. Pediatr Blood Cancer 2015; 62:440–4.
7. Eisinger-Mathason TS, Mucaj V, Biju KM, Nakazawa MS, Gohil M, Cash TP, et al. Deregulation of the Hippo pathway in soft-tissue sarcoma promotes FOXM1 expression and tumorigenesis. Proc Natl Acad Sci U S A 2015;112: E3402–11.
8. Tremblay AM, Missiaglia E, Galli GG, Hettmer S, Urcia R, Carrara M, et al. The hippo transducer YAP1 transforms activated satellite cells and is a potent effector of embryonal rhabdomyosarcoma formation. Cancer Cell 2014;26:273–87.
9. Crose LE, Galindo KA, Kephart JG, Chen C, Fitamant J, Bardeesy N, et al. Alveolar rhabdomyosarcoma-associated PAX3-FOXO1 promotes tumorigenesis via Hippo pathway suppression. J Clin Invest 2014;124:285–96.
10. Helias-Rodzewicz Z, Perot G, Chibon F, Ferreira C, Lagarde P, Terrier P, et al. YAP1 and VGLL3, encoding two cofactors of TEAD transcription factors, are amplified and overexpressed in a subset of soft tissue sarcomas. Genes Chromosomes Cancer 2010;49:1161–71.
11. Kelleher FC, Viterbo A. Histologic and genetic advances in refining the diagnosis of "undifferentiated pleomorphic sarcoma". Cancers 2013;5: 218–33.
12. Rubin BP, Nishijo K, Chen HI, Yi X, Schuetze DP, Pal R, et al. Evidence for an unanticipated relationship between undifferentiated pleomorphic sarcoma and embryonal rhabdomyosarcoma. Cancer Cell 2011;19:177–91.
13. Wang H, Garzon R, Sun H, Ladner KJ, Singh R, Dahlman J, et al. NF-kappaB-YY1-miR-29 regulatory circuitry in skeletal myogenesis and rhabdomyosarcoma. Cancer Cell 2008;14:369–81.
14. Watt KI, Judson R, Medlow P, Reid K, Kurth TB, Burniston JG, et al. Yap is a novel regulator of C2C12 myogenesis. Biochem Biophys Res Commun 2010;393:619–24.
15. Ciarapica R, De Salvo M, Carcarino E, Bracaglia G, Adesso L, Leoncini PP, et al. The Polycomb group (PcG) protein EZH2 supports the survival of PAX3-FOXO1 alveolar rhabdomyosarcoma by repressing FBXO32 (Atrogin1/MAFbx). Oncogene 2014;33:4173–84.
16. Bakkar N, Wang J, Ladner KJ, Wang H, Dahlman JM, Carathers M, et al. IKK/NF-kappaB regulates skeletal myogenesis via a signaling switch to inhibit differentiation and promote mitochondrial biogenesis. J Cell Biol 2008; 180:787–802.
17. Kadoch C, Crabtree GR. Reversible disruption of mSWI/SNF (BAF) complexes by the SS18-SSX oncogenic fusion in synovial sarcoma. Cell 2013;153:71–85.
18. Nakazawa MS, Eisinger-Mathason TS, Sadri N, Ochocki JD, Gade TP, Amin RK, et al. Epigenetic re-expression of HIF-2alpha suppresses soft tissue sarcoma growth. Nat Commun 2016;7:10539.
19. Tzimas C, Michailidou G, Arsenakis M, Kieff E, Mosialos G, Hatzivassiliou EG. Human ubiquitin specific protease 31 is a deubiquitinating enzyme implicated in activation of nuclear factor-kappaB. Cell Signal 2006;18:83–92.

Downloaded from http://aacrjournals.org/cancerres/article-pdf/78/10/2705/2764759/2705.pdf by guest on 27 August 2022

20. Subramanian A, Tamayo P, Mootha VK, Mukherjee S, Ebert BL, Gillette MA, et al. Gene set enrichment analysis: a knowledge-based approach for interpreting genome-wide expression profiles. Proc Natl Acad Sci U S A 2005;102:15545–50.
21. Li B, Dewey CN. RSEM: accurate transcript quantification from RNA-Seq data with or without a reference genome. BMC Bioinformatics 2011; 12:323.
22. Robinson MD, McCarthy DJ, Smyth GK. edgeR: a Bioconductor package for differential expression analysis of digital gene expression data. Bioinformatics 2010;26:139–40.
23. Judson RN, Tremblay AM, Knopp P, White RB, Urcia R, De Bari C, et al. The Hippo pathway member Yap plays a key role in influencing fate decisions in muscle satellite cells. J Cell Sci 2012;125(Pt 24):6009–19.
24. Mito JK, Riedel RF, Dodd L, Lahat G, Lazar AJ, Dodd RD, et al. Cross species genomic analysis identifies a mouse model as undifferentiated pleomorphic sarcoma/malignant fibrous histiocytoma. PLoS One 2009;4:e8075.
25. Kirsch DG, Dinulescu DM, Miller JB, Grimm J, Santiago PM, Young NP, et al. A spatially and temporally restricted mouse model of soft tissue sarcoma. Nat Med 2007;13:992–7.
26. Serrano C, Romagosa C, Hernandez-Losa J, Simonetti S, Valverde C, Moline T, et al. RAS/MAPK pathway hyperactivation determines poor prognosis in undifferentiated pleomorphic sarcomas. Cancer 2016;122:99–107.
27. Wilson AA, Kwok LW, Porter EL, Payne JG, McElroy GS, Ohle SJ, et al. Lentiviral delivery of RNAi for *in vivo* lineage-specific modulation of gene expression in mouse lung macrophages. Mol Ther 2013;21:825–33.
28. Zhou VW, Goren A, Bernstein BE. Charting histone modifications and the functional organization of mammalian genomes. Nat Rev Genet 2011; 12:7–18.
29. Goodwin ML, Jin H, Straessler K, Smith-Fry K, Zhu JF, Monument MJ, et al. Modeling alveolar soft part sarcomagenesis in the mouse: a role for lactate in the tumor microenvironment. Cancer Cell 2014;26:851–62.
30. Deng X, Xu M, Yuan C, Yin L, Chen X, Zhou X, et al. Transcriptional regulation of increased CCL2 expression in pulmonary fibrosis involves nuclear factor-kappaB and activator protein-1. Int J Biochem Cell Biol 2013;45:1366–76.
31. Chang TP, Vancurova I. Bcl3 regulates pro-survival and pro-inflammatory gene expression in cutaneous T-cell lymphoma. Biochim Biophys Acta 2014;1843:2620–30.
32. Kastrati I, Canestrari E, Frasor J. PHLDA1 expression is controlled by an estrogen receptor-NFkappaB-miR-181 regulatory loop and is essential for formation of ER+ mammospheres. Oncogene 2015;34:2309–16.
33. Natarajan K, Singh S, Burke TR Jr, Grunberger D, Aggarwal BB. Caffeic acid phenethyl ester is a potent and specific inhibitor of activation of nuclear transcription factor NF-kappa B. Proc Natl Acad Sci U S A 1996;93:9090–5.
34. Ohtsu N, Nakatani Y, Yamashita D, Ohue S, Ohnishi T, Kondo T. Eva1 maintains the stem-like character of glioblastoma-initiating cells by activating the noncanonical NF-kappaB signaling pathway. Cancer Res 2016; 76:171–81.
35. Berger N, Ben Bassat H, Klein BY, Laskov R. Cytotoxicity of NF-kappaB inhibitors Bay 11-7085 and caffeic acid phenethyl ester to Ramos and other human B-lymphoma cell lines. Exp Hematol 2007;35:1495–509.
36. Payne CM, Weber C, Crowley-Skillicorn C, Dvorak K, Bernstein H, Bernstein C, et al. Deoxycholate induces mitochondrial oxidative stress and activates NF-kappaB through multiple mechanisms in HCT-116 colon epithelial cells. Carcinogenesis 2007;28:215–22.
37. Loganathan SN, Tang N, Fleming JT, Ma Y, Guo Y, Borinstein SC, et al. BET bromodomain inhibitors suppress EWS-FLI1-dependent transcription and the IGF1 autocrine mechanism in Ewing sarcoma. Oncotarget 2016;7: 43504–17.
38. Nielsen TO, Poulin NM, Ladanyi M. Synovial sarcoma: recent discoveries as a roadmap to new avenues for therapy. Cancer Discov 2015;5:124–34.
39. Lee DH, Qi J, Bradner JE, Said JW, Doan NB, Forscher C, et al. Synergistic effect of JQ1 and rapamycin for treatment of human osteosarcoma. Int J Cancer 2015;136:2055–64.
40. Mazur PK, Herner A, Mello SS, Wirth M, Hausmann S, Sanchez-Rivera FJ, et al. Combined inhibition of BET family proteins and histone deacetylases as a potential epigenetics-based therapy for pancreatic ductal adenocarcinoma. Nat Med 2015;21:1163–71.
41. Loven J, Hoke HA, Lin CY, Lau A, Orlando DA, Vakoc CR, et al. Selective inhibition of tumor oncogenes by disruption of super-enhancers. Cell 2013;153:320–34.
42. Ye S, Eisinger-Mathason TS. Targeting the Hippo pathway: Clinical implications and therapeutics. Pharmacol Res 2016;103:270–8.
43. Roudier E, Chapados N, Decary S, Gineste C, Le Bel C, Lavoie JM, et al. Angiomotin p80/p130 ratio: a new indicator of exercise-induced angiogenic activity in skeletal muscles from obese and non-obese rats? J Physiol 2009;587(Pt 16):4105–19.
44. Troyanovsky B, Levchenko T, Mansson G, Matvijenko O, Holmgren L. Angiomotin: an angiostatin binding protein that regulates endothelial cell migration and tube formation. J Cell Biol 2001;152:1247–54.
45. Detwiller KY, Fernando NT, Segal NH, Ryeom SW, D'Amore PA, Yoon SS. Analysis of hypoxia-related gene expression in sarcomas and effect of hypoxia on RNA interference of vascular endothelial cell growth factor A. Cancer Res 2005;65:5881–9.
46. Wang W, Li N, Li X, Tran MK, Han X, Chen J. Tankyrase Inhibitors target YAP by stabilizing angiomotin family proteins. Cell Rep 2015;13:524–32.
47. Zhao B, Li L, Lu Q, Wang LH, Liu CY, Lei Q, et al. Angiomotin is a novel Hippo pathway component that inhibits YAP oncoprotein. Genes Dev 2011;25:51–63.
48. Zambrano S, De Toma I, Piffer A, Bianchi ME, Agresti A. NF-kappaB oscillations translate into functionally related patterns of gene expression. Elife 2016;5:e09100.
49. Tubaro C, Arcuri C, Giambanco I, Donato R. S100B protein in myoblasts modulates myogenic differentiation via NF-kappaB-dependent inhibition of MyoD expression. J Cell Physiol 2010;223:270–82.
50. Penn BH, Bergstrom DA, Dilworth FJ, Bengal E, Tapscott SJ. A MyoD-generated feed-forward circuit temporally patterns gene expression during skeletal muscle differentiation. Genes Dev 2004;18:2348–53.
51. Guttridge DC, Mayo MW, Madrid LV, Wang CY, Baldwin AS Jr. NF-kappaB-induced loss of MyoD messenger RNA: possible role in muscle decay and cachexia. Science 2000;289:2363–6.
52. Perez-Rosado A, Artiga M, Vargiu P, Sanchez-Aguilera A, Alvarez-Barrientos A, Piris M. BCL6 represses NFkappaB activity in diffuse large B-cell lymphomas. J Pathol 2008;214:498–507.
53. Braun T, Gautel M. Transcriptional mechanisms regulating skeletal muscle differentiation, growth and homeostasis. Nat Rev Mol Cell Biol 2011;12: 349–61.
54. Reynaud EG, Leibovitch MP, Tintignac LA, Pelpel K, Guillier M, Leibovitch SA. Stabilization of MyoD by direct binding to p57(Kip2). J Biol Chem 2000;275:18767–76.
55. Lockhart PJ, Hulihan M, Lincoln S, Hussey J, Skipper L, Bisceglio G, et al. Identification of the human ubiquitin specific protease 31 (USP31) gene: structure, sequence and expression analysis. DNA Seq 2004;15:9–14.

Downloaded from http://aacrjournals.org/cancerres/article-pdf/78/10/2705/2764759/2705.pdf by guest on 27 August 2022